

SurEau: a mechanistic model of plant water relations under extreme drought

Hervé Cochard, François Pimont, Julien Ruffault, Nicolas Martin-StPaul

▶ **To cite this version:**

Hervé Cochard, François Pimont, Julien Ruffault, Nicolas Martin-StPaul. SurEau: a mechanistic model of plant water relations under extreme drought. Annals of Forest Science, 2021, 78 (2), pp.55. 10.1007/s13595-021-01067-y . hal-03269429

HAL Id: hal-03269429
https://hal.inrae.fr/hal-03269429

Submitted on 20 Jun 2022

HAL is a multi-disciplinary open access archive for the deposit and dissemination of scientific research documents, whether they are published or not. The documents may come from teaching and research institutions in France or abroad, or from public or private research centers.

L'archive ouverte pluridisciplinaire **HAL**, est destinée au dépôt et à la diffusion de documents scientifiques de niveau recherche, publiés ou non, émanant des établissements d'enseignement et de recherche français ou étrangers, des laboratoires publics ou privés.

Annals of Forest Science (2021) 78: 55
https://doi.org/10.1007/s13595-021-01067-y

RESEARCH PAPER

SurEau: a mechanistic model of plant water relations under extreme drought

Hervé Cochard[1] · François Pimont[2] · Julien Ruffault[2] · Nicolas Martin-StPaul[2]

Received: 8 January 2021 / Accepted: 5 May 2021 / Published online: 14 June 2021
© The Author(s) 2021

Abstract

• ***Key message*** **A new process-based model, *SurEau*, is described. It predicts the risk of xylem hydraulic failure under drought.**
• ***Context*** The increase in drought intensity due to climate change will accentuate the risk of tree mortality. But very few process-based models are currently able to predict this mortality risk.
• ***Aims*** We describe the operating principle of a new mechanistic model *SurEau* that computes the water balance, water relations, and hydraulics of a plant under extreme drought.
• ***Methods*** *SurEau* is based on the formalization of key physiological processes of plant response to water stress. The hydraulic and hydric functioning of the plant is at the core of this model, which focuses on both water flows (i.e., hydraulic) and water pools (i.e., hydric) using variable hydraulic conductances. The model considers the elementary flow of water from the soil to the atmosphere through different plant organs that are described by their symplasmic and apoplasmic compartments. For each organ, the symplasm is described by a pressure-volume curve and the apoplasm by its vulnerability curve to cavitation. The model is evaluated on mature oak trees exposed to water stress.
• ***Results*** On the tested oak trees, the model captures well the observed soil water balance, water relations, and level of embolism. A sensitivity analysis reveals that the level of embolism is strongly determined by air VPD and key physiological traits such as cuticular transpiration, resistance to cavitation, and leaf area.
• ***Conclusion*** The process-based *SurEau* model offers new opportunities to evaluate how different species or genotypes will respond to future climatic conditions.

Keywords Water stress · Hydraulic · Cavitation · Tree · Mortality · Climate change

Handling Editor: Erwin Dreyer

Contribution of the co-authors HC and NM conceptualized the model, with inputs from FP and JR. HC wrote the C code for the model and ran the simulations. JR and NM provided the climatic data. HC and NM wrote the first draft of the manuscript. FP and JR revised and edited the manuscript.

✉ Hervé Cochard
herve.cochard@inrae.fr

François Pimont
Francois.pimont@inrae.fr

Julien Ruffault
julien.ruff@gmail.com

Nicolas Martin-StPaul
nicolas.martin@inrae.fr

[1] Université Clermont Auvergne, INRAE, PIAF, 63000 Clermont-Ferrand, France

[2] INRAE, URFM, 84000 Avignon, France

1 Introduction

Numerous models have been developed to simulate the water relations and gas exchanges of plants under well-watered or limiting hydric conditions (Sperry et al. 1998; Venturas et al. 2018; Mackay et al. 2012; Christofforsen et al. 2016; Tuzet et al. 2017; De Cáceres et al. 2021). These models are based either on empirical relationships or on more mechanistic bases, i.e., based on a physical representation of the physiological processes. A few years ago, we identified that there were few mechanistic models taking into account the water relations of plants under conditions of extreme water stress, i.e., when the plant reaches its survival limit (Xu et al. 2016; Venturas et al. 2018). However, the current context of increasing forest die-off and disturbances in response to climate change–induced drought calls for the development of such a model. This is the reason why we began developing such a

model in 2015, first in a preliminary form in an Excel spreadsheet, then as a R script (Martin-StPaul et al. 2017). These earlier versions used a quasi-static approach, and the plant was limited to two compartments (one symplasmic and one apoplasmic). From 2017 onwards, we developed a new dynamic version of this model, based on a plant segmentation in different organs and implemented in the C programming language. This model has already been used in a number of recent studies (Martin-StPaul et al. 2017, 2020; Scoffoni et al. 2018; Duursma et al. 2019; Cochard 2020a; Brodribb et al. 2019; Brodribb et al. 2020; Dayer et al. 2020; Lamarque et al. 2020; Lopez et al. 2021), but never formally described as here.

The most innovative aspect of this model is its ability to describe the temporal variation of a plant's water status (water potential and water content) beyond the point of stomatal closure. Under these extreme stress conditions, the model simulates the residual transpiration flow through the cuticle, cavitation processes, and the solicitation of the plant's water reservoirs. Hence, the model allows tracking water quantities in the different plant organs and compartments. The objective is also to model these processes both for plants under controlled conditions, as well as under natural current and future conditions. The *SurEau* model is primarily a hydraulic model computing water flows. It can be combined with simplified photosynthesis, energy budget, and growth modules, but those are not described here.

The soil-plant-atmosphere system is segmented and described using different linked hydraulic organ compartments exchanging water fluxes called computational cells, or simply "cells" (Fig. 1). These fluxes are determined by gradients of water potential between cells and hydraulic conductances of these cells. The water quantity of each cell is therefore described as a result of incoming and outgoing fluxes; and the water potential of each cell is computed with the appropriate formulation according to the nature of these cells (soil, symplasm, apoplasm): (i) a water retention curve for the soil (Van Genuchten 1980); (ii) a pressure-volume curve for the symplasm (Tyree and Hammel 1972), which expresses the relationship between water content and water potential; and (iii) a vulnerability curve to cavitation and the capacitance in the case for the apoplasm (Cruiziat et al. 2002). In order to explicitly model the dynamics of the system, the model is integrated over a very small time step (*dt*), on the order of milliseconds, to avoid numerical instabilities associated with the Courant-Friedrichs-Lewy condition (CFL, Dutykh 2016).

In this paper, we aim to (1) provide a full description of the model principles and equations, (2) show typical outputs simulation, (3) demonstrate the ability of the model to simulate key hydraulic variables under extreme drought (water potential, embolism) using a validation dataset collected on an extreme drought experiment on temperate oak (Cochard et al. 1992), and (4) show the sensitivity of key model outputs to future climate and to trait plasticity in response to elevated CO_2.

However, this paper is not a user guide, which can be provided upon request by the corresponding author. An object-oriented open version embedded into the *Capsis* platform (Dufour-Kowalski et al. 2012) is also under development: http://capsis.cirad.fr/capsis/help_en/sureau.

2 Materials and methods

2.1 Model description

2.1.1 Formalization of the soil-plant-atmosphere system in *SurEau*

The soil-plant-atmosphere continuum is idealized as a collection of five linked organ types (roots, trunk, branches, buds, leaves), each of them containing both an apoplasmic and a symplasmic compartment (Fig. 1). In addition, roots and leaves also respectively include an endoderm and an evaporative site. Each compartment is a computational cell of the model. The root system is divided into 3 sub-root systems, each occupying a different soil layer and being connected to the trunk. The crown of the tree is divided into *n* identical branches connected from the trunk in parallel. Therefore, the number of branches has no incidence on the water transport to the canopy that can still be treated using the "big leaf" approximation, unless some forcing variability is considered within the crown.

The state variables for each compartment are presented in Table 1. They include the water potentials (P), osmotic potential (π), turgor pressure (Tp), and the water quantity (Q). Capacitances (C) and conductance (K) are parameters that can vary with temperature, cavitation level in xylem vessels, and leaf fall (Table 2). Hence, the percent loss of conductance (PLC) and the percent leaf fall (PLF) are also considered state variables (Table 1). A simplified representation of the system is presented in Appendix Fig. 7 and a more detailed representation in Fig. 1. In the following, the indices refer to the different compartments or organs. For organs, we use L for leaf, B for branches, bud for bud, T for trunk, and R for roots. As there may be several roots or branches in parallel, we also use index numbers 1, 2,...*n* to designate the organ/number/soil layer. For the compartments, we use indices *apo* or *symp* to designate the apoplasm and symplasm respectively. For roots, the endoderm is designated by the index *endo*. Thus, for example, the water potential of the leaf apoplasm is written $P_{\mathrm{L.apo}}$.

Specificities of the water flows in leaves are shown in Fig. 1B. Sap at pressure $P_{\mathrm{L.apo}}$ enters the leaf through the apoplasm conductance (petioles + veins, $K_{\mathrm{L.apo}}$), then passes through mesophyll cells ($K_{\mathrm{L.symp1}}$) to reach the evaporative site in the substomatic chamber ($P_{\mathrm{L.evapo}}$). This evaporative site is considered an apoplasmic

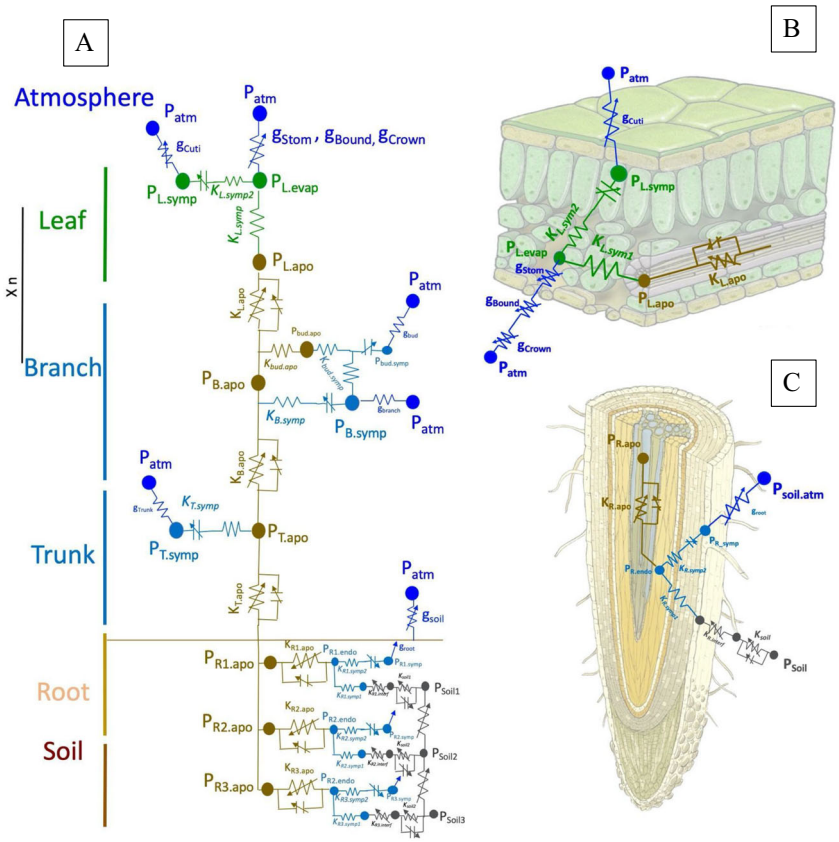


Fig. 1 Idealization of the soil-plant-atmosphere continuum in the modelling framework of *SurEau*. The plant is described as a network of conductances and capacitances. **A** represented the whole architecture of the model. **B** and **C** show the formalizations for leaves and roots, respectively

compartment. The water reservoir of the leaf symplasm is connected through another symplasmic conductance ($K_{L.symp2}$) to the evaporative site. This reservoir also directly loses water via cuticular transpiration. For the roots, we consider a formalism quite similar to leaves (Fig. 1C). For each root, water from the soil reservoir at P_{soil} passes through the soil conductance (K_{soil}), the soil-root interface $K_{R.inter}$, and the cortical symplasmic layer of the absorbent roots $K_{R.symp1}$ to reach the endoderm ($P_{R.endo}$) and then the apoplasm of the root stele ($K_{R.apo}$ to $P_{R.apo}$). The root symplasmic water reservoir is connected to the endoderm by a conductance $K_{R.symp2}$ which can also lose water by evaporation through the root periderm. The three root systems are directly connected in parallel to the trunk. Therefore, $P_{R1.apo} = P_{R2.apo} = P_{R3.apo} = P_{R.apo}$.

We preferred to use *mol* as a unit for water movements (instead of *g* or m^3) for consistency with the gaseous water flows through the stomata or cuticle. The list of parameters and variables used in this article is presented in Table 2.

2.1.2 Implementation of *SurEau*

The general principles of calculating flows and potentials in *SurEau* are the following:

1. Differences in water potentials between compartments create elementary water movement of water molecules (*dq*) at the different interfaces according to fluxes determined from Fick's law using the interface conductance.

Table 1 State variables (that characterize the state of the soil-plant system) used in *SurEau*

State variables	Description	Unit	Type of "cell"
Q	Water quantity	mmol	Apoplasm, symplasm
P	Water potential	MPa	Apoplasm, symplasm
π	Osmotic potential	MPa	Symplasm
Tp	Turgor pressure	MPa	Symplasm
PLC	Percent loss of conductance	%	Apoplasm
PLF	Percent leaf fall	%	-

Table 2 Nomenclature (model variables and parameters used in this document)

Plant	C	Capacitance (specific to apoplasm)	mmol MPa^{-1}
	$\mathcal{E}$	Modulus of elasticity	MPa
	$\pi 0$	Osmotic potential at full turgor (specific to symplasm)	MPa
	P50	Water potential causing 50% cavitation in the xylem	MPa
	Slope	Slope of the curve at P50	% MPa^{-1}
	k	Specific conductivity (is defined between compartments)	$mmol.MPa^{-1}m^2s^{-1}$
	K	Conductance (k times the surface exchange area)	$mmol.MPa^{-1}s^{-1}$
	LAI	Leaf area index	$m^2\ m^{-2}$
	Area	Developed area of the organ considered	m^2
	E	Transpiration rate	$mmol.m^2.s^{-1}$
	g_{canopy}	Canopy conductance	$mmol.m^2.s^{-1}$
	g_{crown}	Crown conductance	$mmol.m^2.s^{-1}$
	g_{bound0}	Reference leaf boundary layer conductance	$mmol.m^2.s^{-1}$
	g_{bound}	Leaf boundary layer conductance	$mmol.m^2.s^{-1}$
	g_{stom}	Stomatal conductance	$mmol.m^2.s^{-1}$
	$g_{stom\text{-}max}$	Maximal stomatal conductance	$mmol.m^2.s^{-1}$
	$g_{stom300}$	Stomatal conductance at a reference $[CO_2]$ of 300 ppm	$mmol.m^2.s^{-1}$
	g_{stom_PAR}	Stomatal response to PAR	-
	δ	Shape parameter of the gs(PAR) relationship	-
	T_{optim}	Temperature at maximal conductance	°C
	T_{sens}	Stomatal conductance sensitivity to temperature	-
	γ	Factor for the regulation of g_{Stom} by turgor loss	-
	Tp_{ref}	Reference turgor pressure for the onset of g_{Stom} regulation	MPa
	frac	Fraction coefficient to compute of Tp_{ref} based on *tlp*	-
	P_{gs12}	Water potential causing 12% stomatal closure	MPa
	P_{gs88}	Water potential causing 88% stomatal closure	MPa
	g_{cuti}	Cuticular conductance	$mmol.m^2.s^{-1}$
	g_{cuti20}	Cuticular conductance at the reference temperature	$mmol.m^2.s^{-1}$
	T_{phase}	Temperature for phase transition of g_{cuti}	°C
	Q_{10a}	Q_{10} values for $g_{cuti} = f(T)$ below T_{phase}	-
	Q_{10b}	Q_{10} values for $g_{cuti} = f(T)$ above T_{phase}	-
	T_{organ}	Organ temperature	°C
	Fluid	Water fluidity (temperature dependent)	-
	OT	Osmotic potential dependence to temperature	-
	ST	Surface tension (temperature dependent)	-
	Rs	Relative water deficit of the symplasm	-
	P_{refill}	Threshold apoplasmic water potential for xylem refilling	MPa
Soil	REW	Relative extractable water	-
	g_{soil}	Soil conductance to water vapor	$mmol.m^{-2}.s^{-1}$
	θ_s	Soil water content at saturation	-
	θ_{fc}	Soil water content at field capacity	-
	θ_r	Soil residual water content	-
	k_{sat}	Soil hydraulic conductivity at saturation	
	α	In verse of the pressure air entry (Van-Genuchten model)	MPa^{-1}
	n	Pore size distribution index (Van-Genuchten equation)	
	l	Shape parameter (Van-Genuchten equation)	
	L_v	Root length per unit soil volume	$m.m^{-3}$
	L_a	Root length per unit soil area	$m.m^{-2}$
	r	Root radius	m
	K_{soil}	Soil hydraulic conductance	

Table 2 (continued)

	ρ	Parameter accentuating the isolation of the root system	
	$K_{R.interf}$	Soil-root interface hydraulic conductance	
Ambiant	T	Temperature	°C
	PAR	Photosynthetic active radiation	$\mu mol.m^{-2}.s^{-1}$
	e_{sat}	Saturation vapor pressure	kPa
	e	Actual vapor pressure	kPa
	VPD	Vapor pressure deficit	kPa
	Wind	Wind speed	$m.s^{-1}$
	RH	Air relative humidity	%
	P_{atm}	Atmospheric pressure	kPa
	Ca	Air CO_2 concentration	ppm

2. The water content of a compartment is increased by *incoming* fluxes and lowered by *outgoing* fluxes and transpiration, because of the water mass conservation law.
3. The water potential of each apoplasm compartment is derived from the water quantity and capacitance; the water potential of each symplasm compartment is derived from its pressure-volume curve.
4. Transpirations are computed from (1) the vapor pressure deficit at the level of each compartment and (2) the gas-phase conductance which includes the cuticle and the stomatal conductance.

Overall, the model is implemented within two loops according to two time steps:

1. A first loop at a very small time step ($dt \sim 0.01$ s) computing sequentially dq (between the different organs and compartments), Q, P (and Pi and Tp), and K.
2. An external second loop computes processes that are not affected by numerical instabilities and that are longer to compute (i.e., with exponential or power functions). It operates on the time scale of seconds to minutes to reduce computational time and includes:

- Organ transpiration and temperature. For leaf compartment, transpiration and temperature are computed at the leaf surface by using stomatal conductance, leaf cuticular conductance by solving the energy budget. For all other compartments (bud, branch, trunk, root), only transpiration is computed using the gas-phase conductance of the organ (g_{organ}, mostly a cuticular conductance) and assuming that $T_{compartment} = T_{air}$ or $= T_{soil}$ for roots.
- Organ cavitation and redistribution of water released by cavitation within other compartments
- The dependency of some physical properties of water solutions (fluidity, surface tension, osmotic potential) to temperature
- Additional processes (photosynthesis, respiration, growth, leaf rain interception, soil evaporation, etc.) which are not described here

Small time step loop: computation at *dt* (~0.01 s) of *dq*, *Q*, *P*, *K* Exchanges of water molecules between organs and compartments (dq, mmol) during small time steps

These elementary exchanges during dt are computed according to Fick's law (with K and P) that allows computing the water fluxes between compartments. The description is given below for all compartments in the order they are computed in the model.

Leaf

- Water movement from the leaf apoplasm to the evaporative site:

$$dq_{L.apo-L.evap} = dt \times K_{L.symp1} \times \left(P_{L.apo} - P_{L.evap}\right) \quad (1)$$

- Water movement between the evaporative site and the symplasm:

$$dq_{L.symp-L.evap} = dt \times K_{L.symp2} \times \left(P_{L.symp} - P_{L.evap}\right) \quad (2)$$

Branch

- Water movement from the branch apoplasm to the leaf apoplasm:

$$dq_{B.apo-L.apo} = dt \times K_{L.apo} \times \left(P_{B.apo} - P_{L.apo}\right) \quad (3)$$

- Water movement from the branch apoplasm to the branch symplasm:

$$dq_{\mathrm{B.apo-B.symp}} = dt \times K_{\mathrm{B.symp}} \times \left(P_{\mathrm{B.apo}} - P_{\mathrm{B.symp}}\right) \quad (4)$$

Trunk

- Water movement from the trunk apoplasm to the branch apoplasm:

$$dq_{\mathrm{T.apo-B.apo}} = dt \times K_{\mathrm{B.apo}} \times \left(P_{\mathrm{T.apo}} - P_{\mathrm{B.apo}}\right) \quad (5)$$

- Water movement from the trunk apoplasm to the trunk symplasm:

$$dq_{\mathrm{T.apo-T.symp}} = dt \times K_{\mathrm{T.symp}} \times \left(P_{\mathrm{T.apo}} - P_{\mathrm{T.symp}}\right) \quad (6)$$

Roots (for root i)

- Water movement from the root apoplasm to the trunk apoplasm:

$$dq_{\mathrm{Ri.apo-T.apo}} = dt \times K_{\mathrm{T.apo}} \times \left(P_{\mathrm{Ri.apo}} - P_{\mathrm{T.apo}}\right) \quad (7)$$

- Water movement from the root endoderm to the root apoplasm:

$$dq_{\mathrm{Ri.endo-R.apo}} = dt \times K_{\mathrm{R1.apo}} \times \left(P_{\mathrm{Ri.endo}} - P_{\mathrm{Ri.apo}}\right) \quad (8)$$

- Water movement from the root symplasm to the root endoderm:

$$dq_{\mathrm{Ri.symp-Ri.endo}} = dt \times K_{\mathrm{Ri.symp2}} \times \left(P_{\mathrm{Ri.symp}} - P_{\mathrm{Ri.endo}}\right) \quad (9)$$

- Water movement from the soil to the root endoderm:

$$dq_{\mathrm{Ri.soil-Ri.endo}} = dt \times \frac{1}{\frac{1}{K_{\mathrm{soili}}} + \frac{1}{K_{\mathrm{Ri.Sympi}}} + \frac{1}{K_{\mathrm{Ri.Interf}}}} \times \left(P_{\mathrm{Soili}} - P_{\mathrm{Ri.endo}}\right) \quad (10)$$

Integration over time of the Water quantity (*Q*, mmol) The integration of elementary variations over small time steps of Q is based on the water mass conservation law following a first-order explicit scheme. It is described below for all compartments as computed in the model. For each compartment interacting with the atmosphere (e.g., evaporative site, symplasm), sink terms corresponding to transpirations (dq_{Stom}, dq_{Cuti}, etc.) are derived from the corresponding gas-phase conductances. These terms are computed in loop 2 (part b.1).

Leaf

- Water content of the evaporative site:

$$Q_{\mathrm{L.evap}} = Q_{\mathrm{L.evap}} + dq_{\mathrm{L.symp-L.evap}} + dq_{\mathrm{L.apo-L.evap}} - dq_{\mathrm{Stom}} \quad (11)$$

with dq_{Stom} the water transpired through the stomata, computed from the stomatal conductance (g_{stom}) and VPD in loop 2.

- Water content of the leaf symplasm:

$$Q_{\mathrm{L.symp}} = Q_{\mathrm{L.symp}} + dq_{\mathrm{L.symp-L.evap}} - dq_{\mathrm{Cuti}} \quad (12)$$

with dq_{Cuti} the water transpired through the leaf cuticle computed from the gas-phase g_{Cuti} and VPD in loop 2.

- Water content of the leaf apoplasm:

$$Q_{\mathrm{L.apo}} = Q_{\mathrm{L.apo}} + dq_{\mathrm{B.apo-L.apo}} - dq_{\mathrm{L.apo-L.evap}} \quad (13)$$

Branch

- Water content of the branch symplasm:

$$Q_{\mathrm{B.symp}} = Q_{\mathrm{B.symp}} + dq_{\mathrm{B.apo-B.symp}} - dq_{\mathrm{Branch}} \quad (14)$$

with dq_{Branch} the water transpired through the branch periderm computed from the gas-phase conductance g_{Branch} and VPD in loop 2.

- Water content of the branch apoplasm:

$$Q_{\mathrm{B.apo}} = Q_{\mathrm{B.apo}} - dq_{\mathrm{B.apo-L.apo}} - dq_{\mathrm{B.apo-B.symp}} + dq_{\mathrm{T.apo-B.apo}} \quad (15)$$

Trunk

- Water content of the trunk symplasm:

$$Q_{\mathrm{T.symp}} = Q_{\mathrm{T.symp}} + dq_{\mathrm{T.apo-T.symp}} - dq_{\mathrm{Trunk}} \quad (16)$$

with dq_{Trunk} the water transpired through the trunk periderm computed from g_{Trunk} and VPD in loop 2.

- Water content of the trunk apoplasm:

$$Q_{\mathrm{T.apo}} = Q_{\mathrm{T.apo}} - dq_{\mathrm{T.apo-B.apo}} - dq_{\mathrm{T.apo-T.symp}} + dq_{\mathrm{R1.apo-T.apo}} + dq_{\mathrm{R2.apo-T.apo}} + dq_{\mathrm{R3.apo-T.apo}} \quad (17)$$

Root

- Water content of the root symplasm:

$$Q_{\mathrm{Ri.symp}} = Q_{\mathrm{Ri.symp}} - dq_{\mathrm{Ri.symp-Ri.endo}} - dq_{Rooti} \quad (18)$$

with dq_{Rooti} the water transpired through the root periderm and computed from the conductance g_{Root1} and VPD in loop 2.

- Water content of the trunk apoplasm:

$$Q_{\mathrm{Ri.apo}} = Q_{\mathrm{Ri.apo}} - dq_{\mathrm{Ri.apo-T.apo}} + dq_{\mathrm{Ri.endo-Ri.apo}} \quad (19)$$

- Water content of the endoderm:

$$Q_{\mathrm{Ri.endo}} = Q_{\mathrm{Ri.endo}} - dq_{\mathrm{Ri.endo-Ri.apo}} + dq_{\mathrm{Ri.symp-Ri.endo}} + dq_{\mathrm{Ri.soil-Ri.endo}} \quad (20)$$

Soil (shown for the first « root layer » over three)

$$Q_{\mathrm{soil.R1}} = Q_{\mathrm{soil.R1}} - dq_{\mathrm{R1.soil-R1.endo}} - dq_{\mathrm{Soil.R1}} + dq_{\mathrm{Soil.R1.R2}} \quad (21)$$

with $Q_{\mathrm{soil.\ R1}}$ soil water content, $dq_{\mathrm{Soil.\ R1}}$ soil evaporation, $dq_{\mathrm{R1.\ soil-R1.\ endo}}$ water transfer between soil and root endoderm, and $dq_{\mathrm{Soil.\ R1.\ R2}}$ capillary transfer between soil layers.

The same equation applies for soil layers two and three. The volume of each soil layer is identical, but the water content of each layer can vary according to its rock fraction.

Water potential (*P*, MPa), osmotic potential (π, MPa), and turgor pressure (*Tp*, MPa) They are computed from the variation in water content, i.e., the difference between the current water content and its value at full saturation (noted with the subscript 0) and organ parameters (C the capacitance, $\mathcal{E}$ modulus of elasticity, and $\pi 0$ the osmotic potential at full turgor). Here, equations are given for the leaf (evaporative site, apoplasm, and symplasm). Similar equations apply for branch, trunk, and roots.

For the *apoplasmic* water potential:

By definition of the capacitance parameters (assumed constant in the apoplasm), we can compute:

- Water potential of the leaf evaporative site:

$$P_{\mathrm{L.evap}} = \frac{Q_{\mathrm{L.evap}} - Q_{\mathrm{L.evap.0}}}{C_{\mathrm{L.evap}}} \quad (22)$$

- Water potential of the leaf apoplasm:

$$P_{\mathrm{L.apo}} = \frac{Q_{\mathrm{L.apo}} - Q_{\mathrm{L.apo.0}}}{C_{\mathrm{L.apo}}} \quad (23)$$

For the *symplasmic* water potential:

The symplasmic water potential is derived from the pressure-volume equations (Tyree and Hammel 1972), it is subsequently defined as the sum of the turgor pressure *Tp* and osmotic potential π

- Water potential of the leaf symplasm:

$$P_{\mathrm{L.symp}} = \pi_{\mathrm{L.symp}} + Tp_{\mathrm{L.symp}} \quad (24)$$

The turgor pressure is computed as:

$$Tp_{\mathrm{L.symp}} = \max\left(0; \pi 0_{\mathrm{L.symp}} x OT_{\mathrm{L}} - \varepsilon_{\mathrm{L.symp}} \times Rs_{\mathrm{L.symp}}\right) \quad (25)$$

with $\pi 0$ the osmotic potential at full turgor, $\mathcal{E}$ the modulus of elasticity, and OT_L is a factor correcting for the effect of temperature on osmotic potential. OT_L is computed at a longer time step, in the second loop. *Rs* is the relative water deficit of the organ symplasm.

$$Rs_{\mathrm{L.symp}} = \frac{Q_{\mathrm{L.symp.0}} - Q_{\mathrm{L.symp}}}{Q_{\mathrm{L.symp.0}}} \quad (26)$$

And the osmotic potential (π) is computed as:

$$\pi_{\mathrm{L.symp}} = \frac{\pi 0_{\mathrm{L.symp}} \times OT_{\mathrm{L}}}{1 - Rs_{\mathrm{L.symp}}} \quad (27)$$

The same equations apply to the symplasm of other organs.

For tall trees, the model also accounts for the gravimetric potential (P_g) due to height (h) as $P_g = -\rho g h$, with ρ the density of water and g the gravimetric constant.

Hydraulic conductances (K, mmol s^{-1} MPa^{-1}) Xylem conductances (apoplasmic) vary from their initial value with the level of cavitation (expressed by the *PLC*, the percent loss in conductivity) and the fluidity of water, which is temperature dependent. In addition to leaf fall and temperature, symplasmic conductances can also depend on other factors, such as the effect of aquaporin regulation. Such additional effects are not described here. Leaf fall (if it occurs) also modifies the leaf conductances. The equation is given here for leaves but the same applies for all organs.

- Conductance of the leaf apoplasm:

$$K_{\mathrm{L_apo}} = K_{\mathrm{L.apo.0}} \times \frac{100 - PLC_{\mathrm{L.apo}}}{100} \times \frac{100 - PLF}{100} \times \mathrm{Fluid_L} \quad (28)$$

- Conductance of the leaf symplasm:

$$K_{\mathrm{L_symp}} = K_{\mathrm{L.symp.0}} \times \frac{100 - PLF}{100} \times \mathrm{Fluid_L} \quad (29)$$

with the $K_{\mathrm{L.\ apo.\ 0}}$ the initial conductance for the leaf apoplasmic compartment, *PLC* the percent loss of conductivity computed from cavitation, *PLF* the percent leaf fall that is empirically derived, and $\mathrm{Fluid_{L.}}$ the water fluidity computed in loop 2.

Large time step loop (1 s or min) This loop computes on a larger time step (*dt*100*, or more) processes that are involved in the update of parameter values and boundary conditions of the system. These computations can be time consuming and are not involved in the constraints associated with the CFL condition, which only deals with water fluxes and time integration of water quantities. It includes transpiration (and energy balance of the leaf), cavitation, and the temperature dependence of some physical properties of water (fluidity, surface tension, osmotic potential). Other processes can be computed in this loop (e.g., photosynthesis, growth) but they do not interact with hydraulics at the time step considered here, so they are not described here.

Transpirations (E,GES mmol s^{-1} m^{-2}) plant loses water through its stomata and its cuticles. The total plant transpiration E_{Plant} can be decomposed as:

$$E_{\mathrm{Plant}} = E_{\mathrm{Leaf}} + E_{Bud} + E_{Branch} + E_{Trunk} + E_{Root} \quad (30)$$

With E_{Leaf} further decomposed as:

$$E_{Leaf} = E_{Stom} + E_{Cuti} \quad (31)$$

Further including the soil water loss E_{soil}, we can compute the "ecosystem" evapotranspiration E_{Eco} as:

$$E_{Eco} = E_{Plant} + E_{Soil} \quad (32)$$

The transpiration E_{organ} (mmol s^{-1} m^{-2}) is computed with the gas-phase conductance g_{organ} (mmol s^{-1} m^{-2}), the vapor pressure deficit between the organ and the atmosphere VPD_{organ} (kPa) and the atmospheric pressure P_{atm} (kPa):

$$E_{\mathrm{organ}} = g_{\mathrm{organ}} \times VPD_{\mathrm{organ}} / P_{\mathrm{atm}} \quad (33)$$

g_{organ} is constant for all organs, except for the cuticle and the stomata, based on specificities described in the next subsections.

The vapor pressure deficit between the air and organ surface is given by:

$$VPD_{\mathrm{organ}} = e_{\mathrm{organ}} - e_{\mathrm{air}} \quad (34)$$

where e_{air} is the vapor pressure of bulk air and e_{organ} is the vapor pressure at the level of the organ symplasm. Both are a function of temperature according to Buck's equation:

$$e_{\mathrm{sat}} = 611.21 \times e^{\left(\left(18.678 - \frac{T}{234.5}\right) \times \left(\frac{T}{T + 257.14}\right)\right)} \quad (35)$$

where T represents either the organ ($e_{\mathrm{sat_organ}}$) or the air ($e_{\mathrm{sat_air}}$) temperature (°C). The leaf temperature is computed from an energy budget model adapted from Sinoquet et al. (2001). The branch, bud, and trunk temperatures are assumed equal to the air temperature. The root temperature is also equal to the soil temperature.

The actual vapor pressure at the level of the compartment under consideration depends on $e_{\mathrm{sat_organ}}$ (kPa) and its water status (P_{organ}, MPa) according to:

$$e_{\mathrm{organ}} = e_{\mathrm{sat_organ}} \times e^{\frac{2.17 \times P_{\mathrm{organ}}}{T_{\mathrm{organ}} + 273.15}} \quad (36)$$

Similarly, the air vapor pressure is a function of air relative humidity *RH* (%):

$$e_{\text{air}} = e_{\text{sat_air}} \times \frac{RH}{100} \tag{37}$$

For root evaporation rates, we compute $e_{\text{air-soil}}$ with the soil water potentials.

Transpiration specificities of the leaf interface (stomata and cuticle):

The conductance of the leaf interface with the atmosphere g_{Canopy} is variable and corresponds to the four following conductances:

- g_{Stom}: the conductance of the stomatal pores
- g_{Cuti}: the conductance of the leaf cuticle

These two conductances are connected in parallel, and the resultant equivalent conductance is in series with:

- g_{Bound}: the conductance of leaf boundary layer
- g_{Crown}: the aerodynamic conductance of the tree crown

The canopy foliage conductance g_{Canopy} is:

$$g_{\text{Canopy}} = \left(\frac{1}{g_{\text{Stom}} + g_{\text{Cuti}}} + \frac{1}{g_{\text{Bound}}} + \frac{1}{g_{\text{Crown}}}\right)^{-1} \tag{38}$$

g_{Bound}, the conductance of the leaf boundary layer, is computed following Jones (2013) and varies with leaf shape, leaf size, and wind speed. For a flat leaf with a characteristic dimension d (m), g_{Bound} can be computed as:

$$g_{\text{Bound}} = 397.2\ \sqrt{\text{Wind}/d} \tag{39}$$

with Wind the wind speed (m.s^{-1}). d is typically taken as the width of the leaf.

g_{Crown}, the conductance of the tree crown, varies only with the wind speed (Jones 2013):

$$g_{\text{Crown}} = g_{\text{Crown0}} \times \text{Wind}^{0.6} \tag{40}$$

with g_{Crown0} the reference conductance and Wind the wind speed (m.s^{-1}).

The conductance of the leaf cuticle g_{Cuti} is a function of the leaf temperature which is based on a single or double Q_{10} equation depending on whether T_{leaf} is above or below the transition phase temperature T_{phase} (Cochard 2020a):

$$\text{if } T_{\text{leaf}} \le T_{\text{phase}} \text{ then} g_{\text{Cuti}} = g_{\text{Cuti_20}} \times Q_{10a}^{\frac{T_{\text{leaf}}-20}{10}} \tag{41a}$$

$$\text{Else}, g_{\text{Cuti}} = g_{\text{Cuti_20}} \times Q_{10a}^{\frac{T_{\text{phase}}-20}{10}} \times Q_{10b}^{\frac{T_{\text{leaf}}-T_{\text{phase}}}{10}} \tag{41b}$$

where $g_{\text{Cuti_20}}$ is the leaf cuticular conductance at 20 °C and Q_{10a} and Q_{10b} are the Q_{10} values of the relationship below and above T_{phase}, respectively.

Once g_{Cuti} is determined, the cuticular transpiration rate E_{Cuti} can be computed as:

$$E_{\text{Cuti}} = \left(\frac{1}{g_{\text{Cuti}}} + \frac{1}{g_{\text{Bound}}} + \frac{1}{g_{\text{Crown}}}\right)^{-1} \times \frac{VPD_{\text{L.symp}}}{P_{\text{atm}}} \tag{42}$$

where $VPD_{\text{L.symp}}$ is computed with a formulation similar to other organs (see above)

Stomatal transpiration is a critical part of the *SurEau* model. It is based on the regulation of stomatal conductance. Several options were implemented to compute this part in the next subsection.

Stomatal transpiration:

Stomatal conductance g_{Stom} is known to respond to multiple variables with the most limiting ones determining the actual conductance (Jarvis 1976). *SurEau* takes into account the dependence of g_{Stom} to light, temperature, and CO_2 concentration on the one hand, and water status on the other. Water status effects are considered through the effect of leaf turgor on g_{Stom}.

First, a maximal stomatal conductance $g_{\text{Stom_max}}$ is defined as a function of g_{Stom} dependence on air temperature (g_{Stom_T}) and to atmospheric CO_2 ($g_{\text{Stom_CO2}}$):

$$g_{\text{Stom_max}} = \left(g_{\text{Stom}_T}; g_{\text{Stom_CO2}}\right) \tag{43}$$

g_{Stom_T} follows a bell-shape temperature response, parametrized with a maximal value at T_{optim} and a sensitivity response to temperature T_{sens}:

$$g_{\text{StomT}} = \frac{g_{\text{Stom_20}}}{1 + \left(\frac{T_{\text{leaf}} - T_{\text{optim}}}{T_{\text{sens}}}\right)^2} \tag{44}$$

where $g_{\text{Stom_20}}$ is the maximal conductance at 20 °C.

$g_{\text{Stom_CO2}}$ depends on atmospheric CO_2 concentration *Ca* (ppm) according to Klein and Raron 2019:

$$g_{\text{Stom_CO2}} = g_{\text{Stom_300}} \times \left(1 + \frac{\partial_{\text{Stom_CO2}}}{100} \times \frac{Ca - 300}{100}\right) \tag{45}$$

with $g_{\text{Stom_300}}$ the $g_{\text{Stom_max}}$ value at 300 ppm and $\partial_{\text{Stom_CO2}}$ a sensitivity parameter (% per 100 ppm). Once $g_{\text{Stom_max}}$ is determined, we use Jarvis's like approach to account for both the effect of incident PAR (μmol m^{-2} s^{-1}) and the effect of water deficit. First, we introduce $g_{\text{Stom_min}}$, the minimum g_{Stom} value when PAR = 0 (Duursma et al. 2019). We then compute $g_{\text{Stom_PAR}}$ as:

$$g_{\text{Stom_PAR}} = g_{\text{Stom_min}} + \left(g_{\text{Stom_max}} - g_{\text{Stom_min}}\right) \times \left(1 - e^{-\delta \times PAR}\right) \tag{46}$$

with δ a shape parameter.

Knowing g_{Stom_PAR}, we can account for the role of water status by assuming that stomata respond to bulk leaf turgor loss. Stomatal conductance decreases with turgor pressure losses, from a reference turgor pressure (Tp_{ref}) at which stomata are considered to be fully open. Technically, this is done by computing a factor γ defined as:

$$\gamma = \frac{Tp_{L.symp}}{Tp_{ref}} \quad (47)$$

then, g_{Stom} is assumed proportional to g_{Stom_PAR} through:

$$g_{Stom} = \gamma . g_{Stom_PAR} \quad (48)$$

where Tp_{ref} can be set equal to the leaf turgor pressure measured at midday on sunny and well-watered conditions. Alternatively, Tp_{ref} can be set at a fraction (frac) of leaf osmotic potential at full turgor ($\pi 0_{L.\ symp}$/frac) to match the observation that the water turgor pressure affects stomatal conductance only below a certain threshold. A major advantage of this approach is that the stomata response to drought can be parameterized using leaf pressure-volume curves equations available for many species (Bartlett et al. 2012; Martin-StPaul et al. 2017). The pressure-volume approach makes also implicit the characterization of the symplasm capacitance.

It is important to note that as $E_{leaf} = E_{Stom} + E_{Cuti}$, transpiration remains lower-bounded by E_{cuti} even when stomata are fully closed with $E_{Stom} = 0$.

For all organs, the elementary water movements dq_{organ} from transpiration are finally computed

$$dq_{organ} = E_{organ} \times Area_{organ} \times dt \quad (49)$$

Cavitation and redistribution of cavitated water The percent loss of conductivity (*PLC*) is computed for the apoplasmic compartments of the different organs with a sigmoidal function. For instance, the *PLC* of a branch at time *t* is:

$$PLC_{Branch} = \frac{100}{1 + e^{\frac{slope_{Branch}}{25} \times \left(P_{B.apo_t} - P50_{Branch} \times ST\right)}} \quad (50)$$

with $P50_{Branch}$, the $P_{B.apo}$ corresponding to a PLC of 50%, and $slope_{Branch}$ the slope of the curve at $P50_{Branch}$ and *ST* a factor accounting for the effect of temperature on water surface tension. By default, xylem refilling under negative pressure does not occur in *SurEau*, and thus, *PLC* can only increase under drought. The *PLC* increases in an organ as soon as the water potential in the apoplasm continues to decrease below cavitation thresholds. When cavitation occurs, some apoplasmic water (dQ_{cavit}) is released in the system in proportion of the *PLC*:

$$dQ_{cavit} = \delta PLC \times Q\text{organ}.0100 \quad (51)$$

where δPLC is the variation of cavitation between the current and previous time steps. dQ_{cavit} is distributed between the adjacent symplasmic and apoplasmic compartments in proportion to their respective hydraulic conductances. It is possible to activate a "refilling option," which allows cavitated conduits to be refilled with surrounding symplasmic water, when the xylem apoplasmic water potential increases above a user-defined threshold (P_{refill}).

Temperature-dependent physical properties Because one objective of *SurEau* was to predict plant water relations during heatwaves, we paid special attention to the temperature dependence of the main physical properties of water solutions (see Cochard 2020a for more details). The reference values of the different parameters are taken at 20 °C.

Fluidity

The dynamic fluidity of liquid water, Fluid, is the reciprocal of its viscosity and varies with temperature according to the empirical formula:

$$Fluid_{organ} = 1.01212 \times 10^{-4} \times T_{organ}{}^{2} + 2.04152 \times 10^{-2} \times T_{organ} + 5.51781 \times 10^{-1} \quad (52)$$

Surface tension of water

The surface tension of liquid water against air decreases with temperature according to this empirical formula:

$$ST_{organ} = \left(75.6986 - 2.6457 \times 10^{-4} \times T_{organ}{}^{2} - 1.4236 \times 10^{-1} \times T_{organ}\right)/72.7455 \quad (53)$$

Osmotic potential temperature dependence

Following van't Hoff relation, we define *OT* as:

$$OT_{organ} = \left(T_{organ} + 273.16\right)/293.16 \quad (54)$$

Soil state variables (P_{soil} and K_{soil} computed for each layer)

The hydraulic properties of the soil layers are defined by pedo-transfer functions following van Genutchen (1980). Accordingly, the soil properties are characterized by 6 parameters (θ_s, θ_r, α, n, K_{sat}, l). We describe the computation only for one layer.

The relative soil water content *REW* is the amount of water available between the water content θ_{fc} at field capacity (P_{soil} = −0.033 MPa) and the residual water content θ_r:

$$REW = \left(\frac{Q_{soil}}{Q_{soil.0}} \times \theta_{fc} - \theta_r\right)/(\theta_s - \theta_r) \quad (55)$$

with θ_s the soil water content at saturation. We assumed that the soil water content cannot be higher than its value at field capacity.

Table 3 Main physiological parameters of the plant organs and compartments

Organs	Parameters	Leaf	Branch	Trunk	Root
Symplasm	$\pi 0$ (MPa)	−2.1	−2.1	−2.1	−2.1
	$\mathcal{E}$ (MPa^{-1})	10	10	10	10
	K (mmol s^{-1} MPa^{-1})	21.0	5.8	2.7	7.0
	Q_0 (mol)	43.7	134.7	354.4	329.3
	Surface (m^2)	10.5	5.8	2.7	54.1
Apoplasm	P50 (MPa)	−3.4	−3.4	−3.4	−3.4
	Slope (% MPa^{-1})	60	60	60	60
	K (mmol s^{-1} MPa^{-1})	31.5	82.5	393.9	3568
	Q_0 (mol)	14.6	269.5	709.0	658.6

The bulk soil water potential at *REW* is given by:

$$P_{\text{soil}} = -\frac{\left(\left(\frac{1}{REW}\right)^{\frac{1}{m}}-1\right)^{\frac{1}{n}}}{\alpha} \text{ and } m = 1-\frac{1}{n} \quad (56)$$

The soil hydraulic conductance at the interface with fine roots is computed as:

$$K_{\text{Soil}} = K_{\text{Sat}} \frac{2\pi L_a}{\ln\left(\frac{1}{r\sqrt{\pi L_v}}\right)} REW^l \times \left[1-\left(1-REW^{1/m}\right)^m\right]^2 \times \text{Fluid}_{\text{soil}} \quad (57)$$

with L_a and L_v the root length per soil area and soil volume, respectively, and r the radius of the roots.

The conductance of the interface between the soil and the root, $K_{\text{R.interf}}$ is empirically computed as a function of the root symplasmic shrinkage by dehydration:

$$K_{\text{R.interf}} = 10 \times K_{\text{Soil}} \times \left[\frac{Q_{\text{R.symp}}}{Q_{\text{R.symp.0}}}\right]^{\rho} \quad (58)$$

with ρ a parameter accentuating the isolation of the root system from the dry soil. The factor 10 expresses that the length of the interface is 10 times shorter than the average length between the root and the soil.

Finally, we compute the evaporation from the soil surface E_{soil} assuming a gaseous conductance g_{soil} of the soil-atmosphere interface depending on the *REW* of the topsoil layer as:

$$E_{\text{soil}} = g_{\text{soil.0}} \times REW_1 \times \frac{VPD_{\text{soil}}}{P_{\text{atm}}} \quad (59)$$

with $g_{\text{soil.0}}$ the conductance at soil saturation.

2.2 Example application: validation data set and sensitivity analysis

To illustrate *SurEau*'s functioning, we performed different simulations using a case study in a young oak forest in eastern France with different data we previously collected (Cochard et al. 1992; Bréda et al. 1993a, 1993b). These trees were exposed to an artificial drought by intercepting rainfall for 3 consecutive years. Other trees were irrigated as controls. Tree morphological parameters were derived from stand characteristics extracted from the references above. On average, the trees were 12.5 m high, with a diameter of 8.6 cm, a leaf area of 10.5 m^2 and occupying each a soil volume of 2 m^3. Tree physiological variables and gaseous phase and soil parameters used in that simulation are given in Tables 3, 4, and 5. These variables were adjusted to correspond to observed daily variations in sap flow and leaf water potentials. Parameters that were not measured were obtained from the literature. The set of parameters used for these simulations is presented in Appendix Table 7.

Overall, we performed four sets of simulations: (1) The first simulation set assumes constant climatic conditions from day to day, but variable diurnally (Table 6). (2) A second set of simulations used actual climate data in the control and rainfall exclusion plots to demonstrate the ability of the model to simulate key hydraulic variables under extreme drought (water potential, embolism). (3) A third set of simulations show the sensitivity of key model outputs to future climate. (4) Finally, a fourth set of simulation show the sensitivity of key model outputs to trait plasticity in response to elevated CO_2 which is a key uncertainty in plant response to climate change.

For the first set of simulations, the plant is initialized in a soil at its field capacity and allowed to dehydrate gradually until being completely dry (water inputs from precipitation are assumed to be equal to zero). g_{Stom} was here modelled with stomata responding to bulk leaf symplasmic turgor potential (Eq. [47]).

Table 4 Main parameters for the flows in gaseous phase

Gas-phase parameters	$g_{\text{Stom_max}}$ (mmol s^{-1} m^{-2})	$g_{\text{Stom_min}}$ (mmol s^{-1} m^{-2})	g_{Cuti} (mmol s^{-1} m^{-2})	T_{phase} (°C)	Q_{10a}	Q_{10b}	g_{Crown} (mmol s^{-1} m^{-2})
Values	200.0	20.0	3.0	37.5	1.2	4.8	45

Table 5 Soil parameters

Soil parameters	Volume (m^3)	θ_s	θ_r	α (cm^{-1})	n	K_{sat} (mmol/s/MPa)	l	Soil depth (m)	RU (mm)	L_a ($m/m^{2)}$	L_v (m/m^3)
Values	2	0.28	0.1	0.0005	2	5.0	0.5	1.12	200	1910	1706

In a second set of simulations, we used actual climatic data from a nearby weather station (Tomblaine, 54) to simulate the drought response of these trees during the 3 years of the experiment (1990). The incoming rainfall was set to zero during the period of rain exclusion. All the model parameters were set constant between the different years, with the only exception of leaf phenology (dates for bud burst and leaf fall).

In a third set of simulations, we used long-term climate data from the Tomblaine weather station and from climate projection models to simulate the inter-annual variation of embolism over the 1950–2010 period under historic and future climate (Fig. 2). For future climate data, we used ALADIN model (Centre National de Recherches Météorologiques, CNRM) for three Radiative Concentration Pathways (RCP2.6, RCP4.5, and RCP8.5) corresponding to the Tomblaine station. At the end of each calendar year, the *PLC* of each organ was set to zero, assuming therefore no legacy from the previous year drought.

In a fourth set of simulations, we performed a model sensitivity analysis to a few key parameters that determine hydraulic failure dynamics under drought. We varied independently each of these traits in the range of −100 to +100% and computed the impact on leaf PLC. Simulations were performed for the last decade of 2100 using climate of the RCP8.5.

3 Results

Simulations were performed with *SurEau* version 20-12-26. Results from the first set of simulations (i.e., constant climate) are shown in Fig. 3 and Appendix Fig. 8. At the beginning of the simulation (Appendix Fig. 8), the daily variations of plant physiological variables follow the daily climatic variations, when the soil is still well-watered. The stomatal conductance is mainly controlled by the light intensity, but the dynamics of transpiration and water potentials are slightly delayed with respect to this conductance because the VPD peak is reached 2 h after solar noon. Note the typical midday stomatal depression. The model, therefore, captures well these complex responses of stomata and transpiration to daily meteorological changes. When dehydration is maintained, the stomata progressively close according to the intensity of foliar water stress (Fig. 3). After about 40 days, the stomata are permanently closed and transpiration is limited to cuticular losses which gradually accentuate the drought stress of the plant. At this stage, cavitation events accentuate in the apoplasm of the different organs, decreasing the amount of water stored in the vessels. When the embolism rate of the leaf apoplasm reaches 100% (after 110 days), the leaf water potential drops abruptly (to reach the air water potential) as leaves lose their symplasmic water stock. The hydraulic failure of the leaf xylem tissue causes desiccation. Later (day 125), the same phenomenon occurs for branches, and finally for the trunk.

Results from the second set of simulations are presented as a validation exercise on an experimental extreme drought. They are presented in Fig. 2 and Fig. 4. They are based on actual climate data from the Tomblaine station. Overall, the model reproduced well the seasonal variations in water potential, soil moisture content, and transpiration of control and stressed trees at the seasonal and daily time scale (Fig. 4). One exception was the transpiration of stressed trees at the beginning of the stress period, which was slightly overestimated (Fig. 4C). The time courses of embolism rates predicted by *SurEau* for the 3 years of experimentation corresponded well with the rates measured in situ (Fig. 2).

The sensitivity of the model—in terms of embolism (*PLC*)—to long-term climate change, both historical and future, is presented in Fig. 5. Before 2020, the predicted embolism rate remains generally low (< 10%), except for particularly dry years when *PLC* could exceed 50% (2003, 2019, 2020). Projected embolism rates for the period 2006–2100 are dependent on the RCP scenario. Under the assumption of RCP2.6, the embolism rate remains on average below 20%. In contrast, under RCP8.5, the embolism rate increases sharply from 2050 to reach nearly 80% towards the end of the century. Over the last two decades of the century, the

Table 6 Climatic conditions

Climatic conditions	$T_{air\text{-}min}$ (°C)	$T_{air\text{-}max}$ (°C)	$RH_{air\text{-}min}$ (%)	$RH_{air\text{-}max}$ (%)	PAR (μmol)	Wind speed (ms^{-1})	VPD_{max} (kPa)
Values	15	30	30	80	1500	1.0	2.97

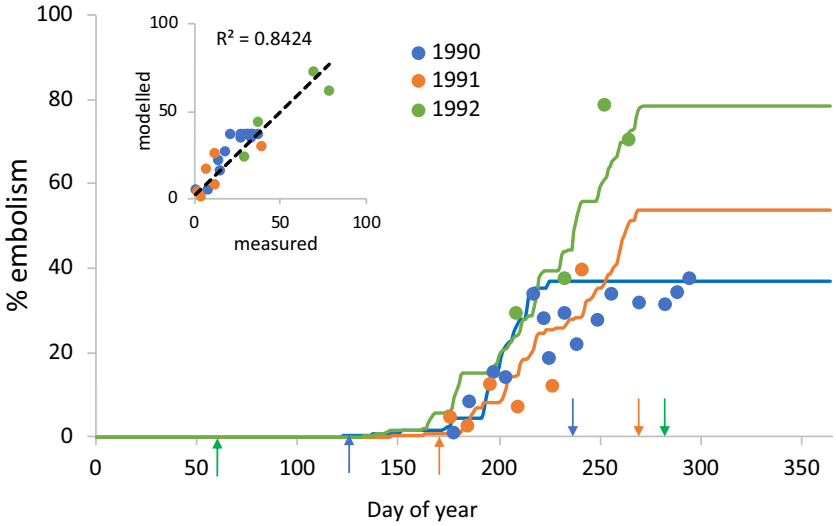


Fig. 2 Observed and modelled degrees of embolism for water-stressed oak trees during three consecutives growing periods. Observed data are shown as dots. The insert shows the correlation between observed and modelled data

embolism rate reaches 100% once every 2 years on average. Projections under assumption RCP4.5 leads to an intermediate between the two aforementioned scenarios. Overall, the inter-annual variability in embolism was strongly correlated with the average daily VPD during the summer period (Fig. 5, insert). High correlations were also found with summer air temperature and humidity (not shown).

Finally, results from the traits sensitivity at the end of the twenty-first century are shown in Fig. 6. Obviously, whereas some traits show a high sensitivity along the sensitivity axis, such as maximal stomatal conductance (g_{stom}) or leaf area (LA) or rooting depth, other traits such as the Q_{10b} or K_{L_symp} show a more limited sensitivity or only within a restricted range. Overall, this sensitivity analysis suggests that maintaining a level of embolism below 50% (maximal level simulated for the recent past decades) requires very strong plasticity for all these traits. For instance, it requires a decrease of LA, g_{stom}, or g_{cuti} by two folds which, if ever it was possible for this oak, would inevitably affect productivity and growth.

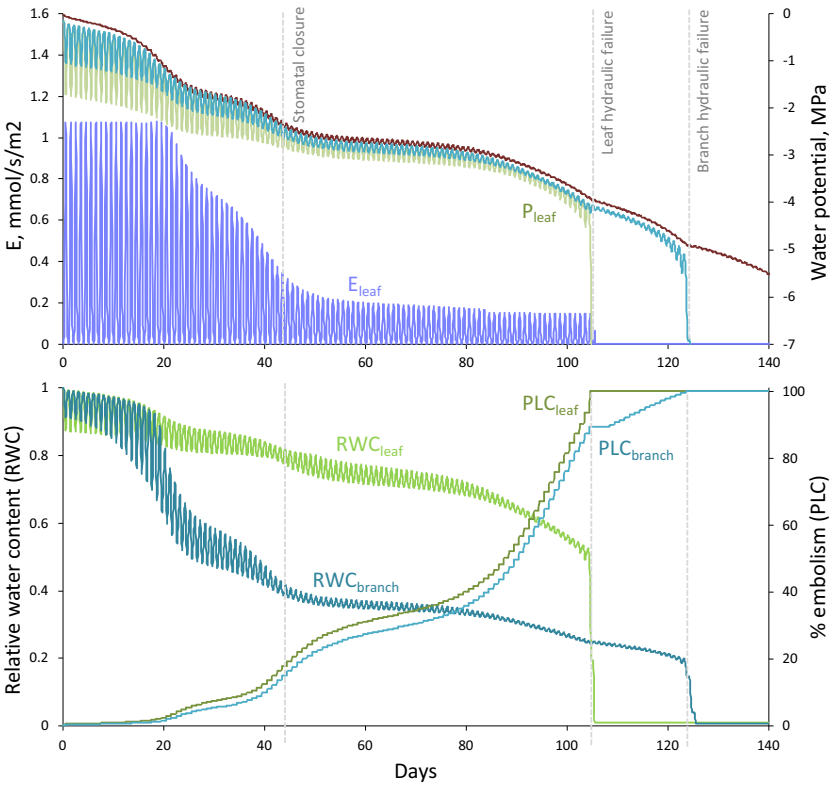


Fig. 3 Simulation of the effect of extreme water stress on different key tree variables during 140 consecutive days. The tree is placed in well-watered soil at $t = 0$ and allowed to dehydrate until complete desiccation. At $t = 44$ days, stomata are closed. At $t = 104$ days, PLC reaches 100% in the leaf apoplasm inducing leaf desiccation, and at $t = 124$ days, hydraulic failure occurs in the branch apoplasm

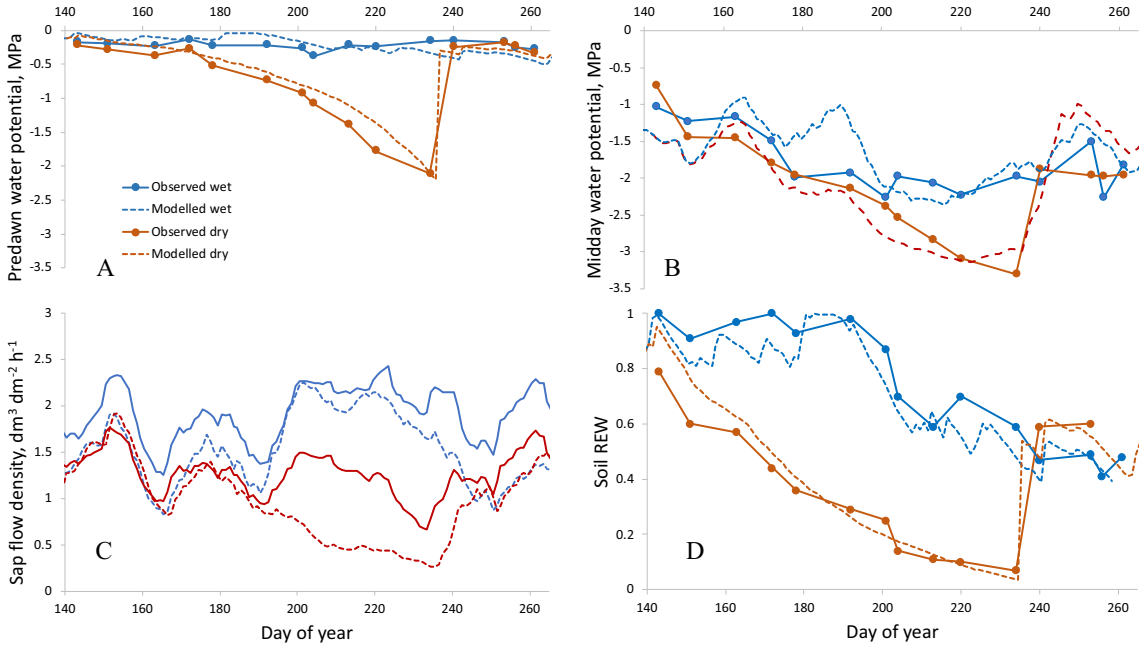


Fig. 4 Observed and modelled seasonal variations of predawn (**A**) and midday (**B**) leaf water potentials, midday sap flow densities (**C**), and soil relative water content (**D**) for well-watered (blue) and water-stressed (red) oak trees during 1990 growing period

4 Discussion

4.1 General about the model

The *SurEau* model uses classic bioclimatic and hydraulic formalisms to account for gas exchanges and the water relations of a plant. This modelling is based on the water mass conservation and on a parameterization of hydraulic and hydric properties of the apoplasmic and the symplasmic properties of organs (roots, trunk, branches, leaves compartments).

This idealization of plants in a few compartments (fine roots, roots, trunk, branches, buds, and leaves) and by separating their symplasm and apoplasm (Fig. 1) offers a good compromise between numerical constraints (mainly the computation time linked to the CFL constraint) and the realism of the representation of the plant for the hydric and hydraulic processes of interest to us, thus both before and after the

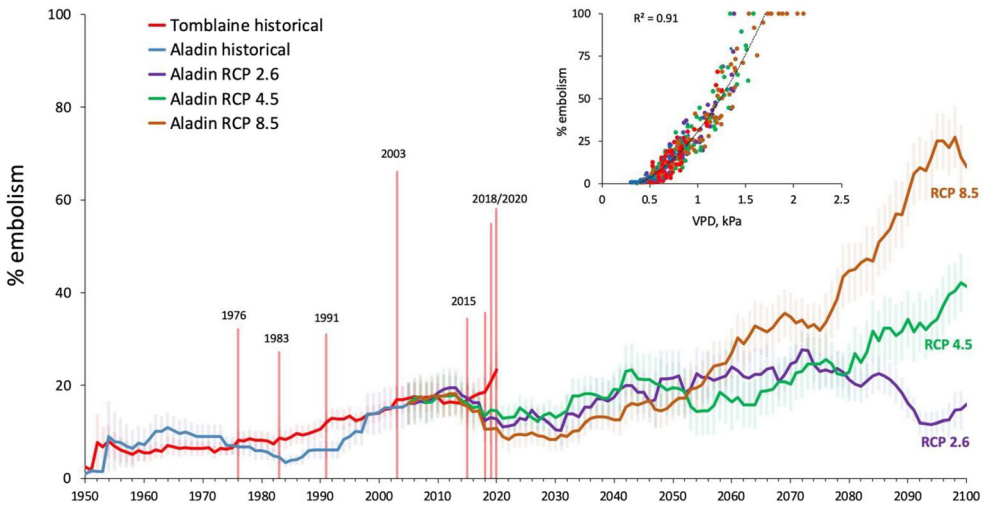


Fig. 5 Prediction of the maximum annual degree of embolism for oak trees under past and future climatic conditions. The red line shows the embolism levels predicted with historical climatic data from a nearby weather station. The vertical red bars represent years with above average embolism and correspond to exceptionally dry events. The other lines show projections of embolism levels based on future climatic scenarios. The line represents 20 years running means, with SE. The correlation between the average daily VPD during the summer period and the modelled PLC is shown in the insert

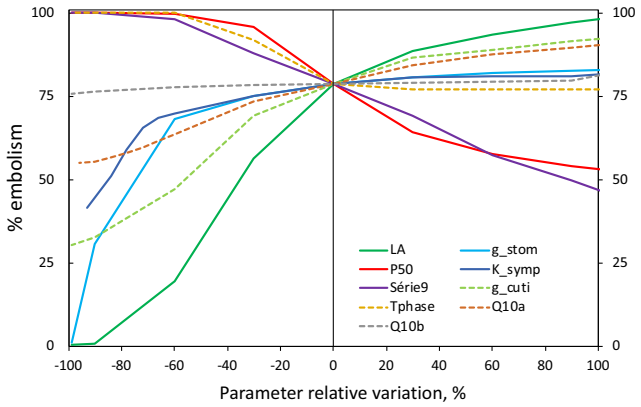


Fig. 6 Sensitivity of *SurEau* predictions to local variations of several key parameters. *SurEau* was used under future climatic conditions (last decades of twenty-first century) by varying the different parameters individually. Embolism (*PLC*) was used as the output variable

stomatal closure (Fig. 3). The number of parameters in the model remains quite high, but a model parameterization in accordance with the field measurements remains possible, as shown in our application example. Indeed, our validation exercise indicates that the model can capture the effect of water stress on the induction of cavitation, and thus on the subsequent hydraulic failure of the xylem on the desiccation of organs fed by this tissue. Consistently, we were able to reproduce the dynamics of cavitation in field trees exposed to extreme drought for 3 years (Fig. 2).

A number of experimental tools—not described here—have been developed and are still under development to estimate the most difficult parameters to measure. For example, a fractal representation of the aerial and root parts allows estimating the volumes and exchange surfaces of these organs.

As stated above, the main limitation of our model is currently its computational cost, an inevitable consequence of our first-order explicit numerical scheme to model dynamic processes, which imposes a very short time step to avoid the numerical instabilities. This well-known numerical constraint is referred to as the CFL (Dutykh 2016). For example, the simulation shown in Fig. 3 required a calculation time of 2 min on a PC with a powerful processor (AMD 2970WX). This execution time is not a constraint to simulate an isolated tree, but can be critical to simulate long climatic series on network grids for instance. To overcome this limitation, other numerical integration techniques of *SurEau* (quasi steady-state approach, hyperbolization of the Durdorf-Frankel scheme as presented in Dutykh 2016) as well as simplified steady-state versions of the models are under development. They would allow speeding up the code and also lowering the parameterization requirements.

4.2 Application to predict drought stress under current and future climate

Predicting the effects of water stress on the functioning of trees, ecosystems, and vegetation is one of the key issues in current ecological research. It is most often based on water balance approaches that are excellent tools for integrating the effects of soil and climate on drought (Rambal 1984; Granier et al. 1999; Ruffault et al. 2013; De Cáceres et al. 2015) but poorly take into account the diversity of plant characteristics and strategies that determine their resistance to drought (Tramblay et al. 2020). The most critical applications of *SurEau* concern understanding and predicting the effects of extreme water stress related to future climate change on plant survival. For that objective, the model simulates both water transport losses due to cavitation and the water content of the organs in particular the living tissue (i.e., the symplasm, Fig. 3). Indeed, loss of hydraulic function due to embolism during extreme drought is a key indicator of drought-induced mortality (Adams et al. 2017), and this process is accurately reproduced by *SurEau* at our study site (Fig. 2). Many current projections of the effects of climate change on vegetation functioning are made with photosynthesis-based models, where the predicted increase in CO_2 triggers an increase in photosynthesis that offsets the effects of drought stress. This formalism generally leads to an increase in end-of-century productivity for many species in many temperate zones (Cheaib et al. 2012), even when plant hydraulics are assumed to constrain the photosynthetic models (Sperry et al. 2019). However, these results are uncertain because alternative modelling methods based on statistical tools tell a very different story, in which the range of trees is expected to shrink strongly due to climate change (Cheaib et al. 2012; Walker et al. 2020). The use of a process-based hydraulic model such as *SurEau* can therefore provide a third perspective on what might happen to trees in the coming decades.

A major advantage of *SurEau* is the ability to integrate the diversity of plant hydraulic traits to determine drying trajectories that are measurable in the laboratory (Martin-StPaul et al. 2017). Indeed, our second simulation series on the oak experiment shows the accuracy of the model for simulating variations in the water status of trees. Ongoing efforts are underway for a broader evaluation of the model in a variety of study sites.

On the basis of such validation, we performed preliminary tests of climate change projections. Accordingly, Fig. 5 suggests that lethal embolism rates could be reached before the end of the century under the worst-case scenario (RCP8.5). From these simulations, it is possible to derive simpler climatic approximations of embolism. As shown in the inset of Fig. 5, the annual average air VPD is a very

good explanatory variable of the embolism level. These results are similar to various experimental results showing close links between mortality and high VPD (William et al. 2013). This relationship is specific to the plant parameters used in these simulations, and could be extended to various species/provenances to assess the spectrum of the potential response of plants to climate change, in terms of embolism.

The embolism projections made with *SurEau* in Fig. 5 should be taken with caution as many processes are not implemented in SurEau, in particular the ability of trees to acclimatize to different aspects of climate change. Among the different facets of climate change, there are large uncertainties in the literature regarding the potential effects of increasing atmospheric CO_2 (Cheaib et al. 2012). However, it is known that an increase in atmospheric CO_2 can trigger the plasticity of certain traits, but there is little data available so far (Domec et al. 2017; Klein and Ramon 2019). In our last simulation exercise, we tried to evaluate the potential effects of trait plasticity on the risk of oak hydraulic failure at the end of the century for the RCP8.5 scenario (900 ppm). The results indicate that the level of plasticity required to limit embolism to historical (non-fatal) levels is very high, and probably unrealistic. But a more global sensitivity analysis of the model remains to be done, as additive effects of several traits are plausible.

4.3 Comparison with other modelling approach

It is now widely recognized that improving predictions of drought impacts requires coupling ecohydrological principles with hydraulic theories and trait-based plant strategies (Tramblay et al. 2020). Consequently, much research is currently focused on improving vegetation models by including the hydraulic framework and hydraulic traits in these models (e.g., Christofforsen et al. 2016; Xu et al. 2016; Tuzet et al. 2017; Venturas et al. 2018; Sperry et al. 2019; De Cáceres et al. 2021; Morin et al. 2021; Li et al. 2021).

There are different categories of plant hydraulics modelling strategies, as recently synthesized (Mencuccini et al. 2019; McDowell et al. 2019; Li et al. 2021). According to the overview provided by Li et al. 2021, SurEau belongs to electrical analogy models (EAMs) that conceptualize water flow through plants as being analogous to the current through an electric circuit with series of resistance and/or capacitance (Sperry et al. 1998). Within the EAM category, SurEau belongs to the resistor-capacitor model type (RCM) as it considers both resistance and water storage (capacitance) as opposed to more simple schemes that only consider resistance, such as the initial version of the model TREE (Loranty et al. 2010; MacKay et al. 2012), the SOX scheme developed by Eller et al. (2018), and the PHS scheme in CLM5 (Kennedy et al. 2019) or the Venturas et al. (2018) approach. The RCM frameworks, which also include plant internal store, have been developed by Sperry et al. (1998), Steppe et al. (2006), MacKay et al. (2012); Gentine et al. (2016), Xu et al. (2016), Christoffersen et al. (2016), Tuzet et al. (2017), and Li et al. (2021). The hydraulic capacitance has indeed been demonstrated to play a critical role in regulating transpiration (Matheny et al. 2015; Huang et al. 2017; Yan et al. 2020), delaying water potential drop (Huang et al. 2017) and may improve desiccation tolerance (Tyree and Yang 1990; Hölttä et al. 2009; Blackman et al. 2016).

The representation of plants in the SurEau model shows some deviations from the recently developed hydraulic-based models used in land surface models. In all RCM-type models previously published, the apoplasmic and symplasmic compartments are not separated, which limits the possibility of explicitly simulating the water content of living tissues. However, living tissue water content is likely to be a key factor in organ and plant mortality (Martinez-Vilalta et al. 2019; Mantova et al. 2021). In SurEau, the specific description of symplasmic and apoplasmic capacitance and resistances between symplasm and apoplasm would allow further understanding of how water transfer fluxes between these compartments can improve survival. This framework also allows the prediction and monitoring of water storage in the plant, which can be expressed per unit volume, surface area, or dry mass, a key factor in ecosystem disturbance such as mortality (Martinez-Vilalta et al. 2019). This also offers promising opportunities for a wide range of applications. These include comparison with remote sensing products for moisture content (Fan et al. 2018; Marino et al. 2020) or promising prediction of moisture content of living fuels for fire risk assessment (Martin-StPaul et al. 2020), which is a critical factor in fire behavior (e.g., Ruffault et al. 2018; Pimont et al. 2019). SurEau also departs by the fact it includes an explicit description of cuticular losses connected to the symplasm of the different plant organs described. This can provide a more realistic view of how plants dry out under extreme drought, including once the leaves are lost. Future testing of the model and comparison with other approaches will be useful in highlighting the most relevant processes and features that should be included in land surface models. SurEau has a high degree of biological realism compare to previous model which offers the opportunity to explore sensitivity to various traits that have not been explored to date.

Appendix

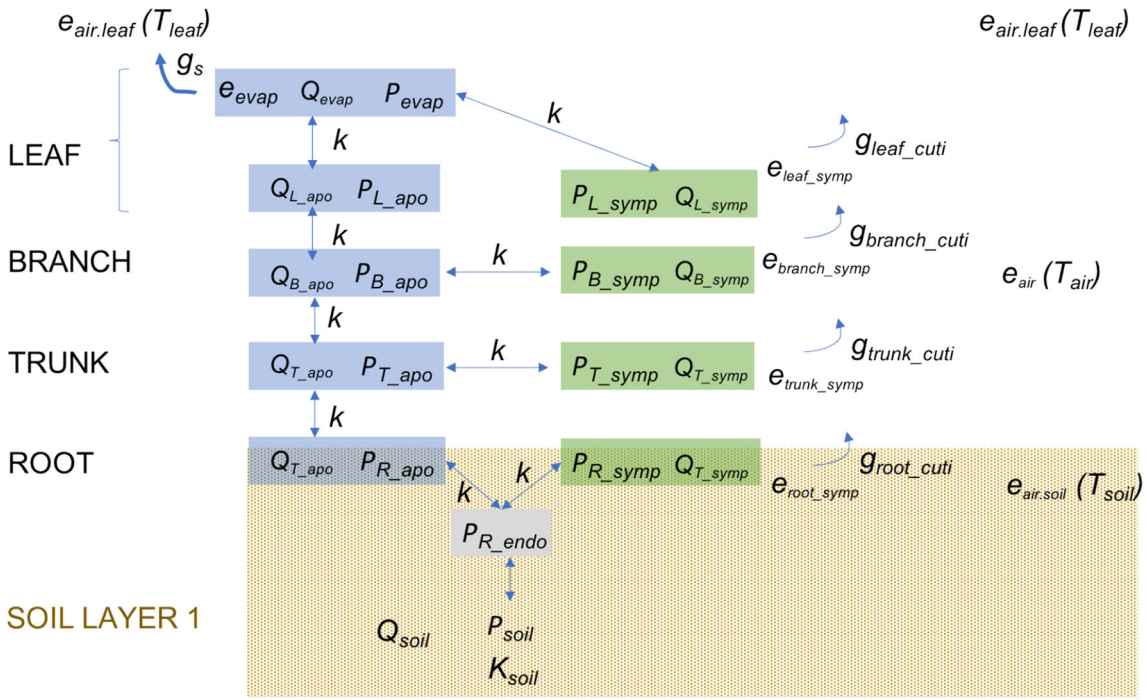


Fig. 7 Simplified representation of the plant architecture in relation to the environment as implemented in the *SurEau* model. *Q* and *P*, the water quantity and water potential defined within a compartment (or "computational cell"); *K*, the hydraulic conductance defined between two compartments (materialized by arrows); *g*, the gas-phase conductance; *e*, the actual vapor pressure; *T*, the temperature

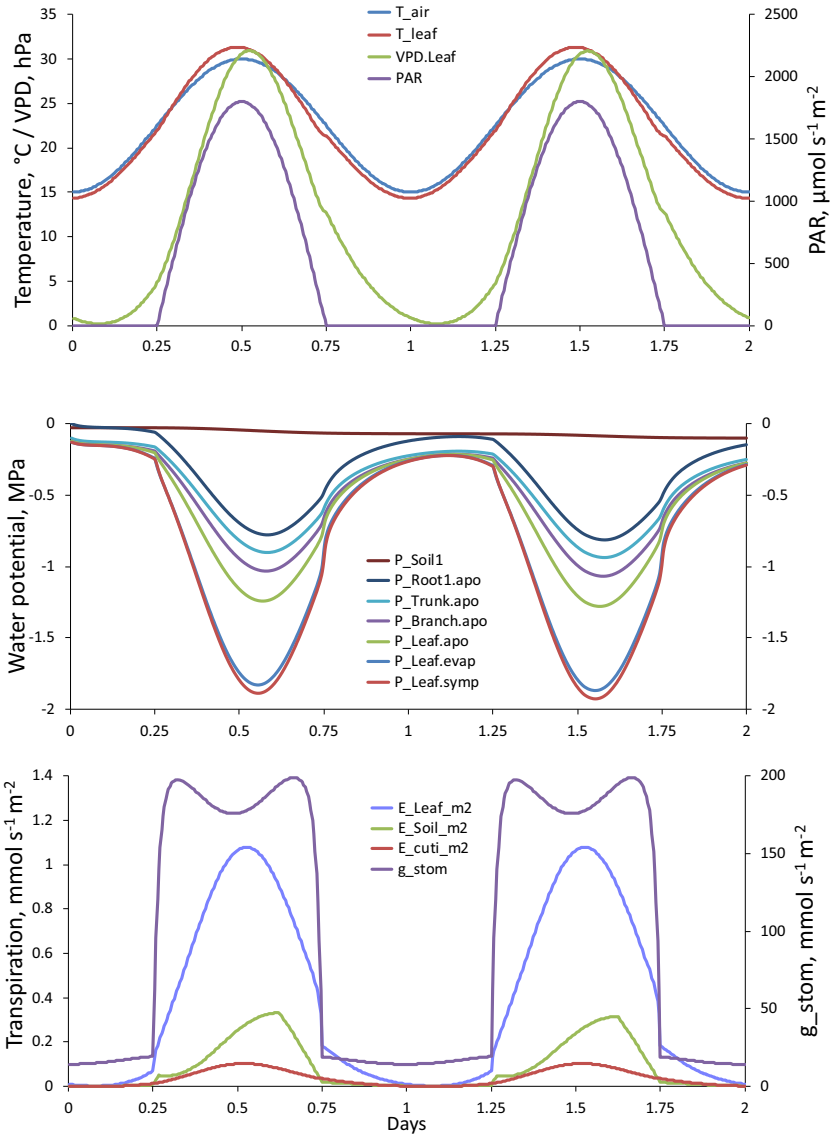


Fig. 8 Daily variations of key physiological variables simulated with *SurEau*. Two consecutive days are simulated for a well-watered plant

Table 7 List of the main parameters of the SurEau model used in for the simulations

Parameters			Name in SurEau	Unit	Value
Soil	Soil depth		*Soil_Depth*	*m*	1,12
	Soil width		*Soil_Width*	*m*	1,32
	Rock fraction	Layer 1	*Rock_f1*	*%*	0
		Layer 2	*Rock_f2*	*%*	0
		Layer 3	*Rock_f3*	*%*	0
	Parameters forvan Genuchten equation	Teta_s	*Teta_s*	*m3/m3*	0,28
		Teta_r	*Teta_r*	*m3/m3*	0,1
		alpha	*alpha*	*cm-1*	5,00E-04
		n	*n*	-	2
		K_sat	*K_sat*	*mol/s/m/MPa*	5
		L	*L*	-	0,5
Rain interception	Minimum interception		*Interception_min*	*%*	20
	Threshold rain intensity		*Threshold_rain*	*mm*	2
	Interception factor		*Interception_factor*	-	1
Leaf	Characteristic size		*Leaf_size*	*mm*	50
	Leaf angle		*leaf_angle*	*degrees*	45
	Maximum leaf area		*LA_max_init*	*m2*	10,5
	Minimum leaf area		*LA_min*	*m2*	0
	Leaf phenology	Day at budburst	*LA_day1*	*DOY*	123
		First day at LA_max	*LA_day2*	*DOY*	140
		Last day at LA_max	*LA_day3*	*DOY*	285
		First day at LA_min	*LA_day4*	*DOY*	325
	Leaf succulence		*Succulence*	*g/m2*	100
	Apoplasmic fraction		*Leaf_apo_fraction*	*%*	0,25
	LMA		*LMA*	*g/m2*	45,85
Branch	Length		*Length_Branch*	*m*	2,5
	Branch end diameter		*Diam_Branch*	*m*	0,003
	Apoplasmic fraction		*Branch_apo_fraction*	*%*	0,4
	Symplasmic fraction		*Branch_symp_fraction*	*%*	0,2
	Density		*Density*	*kg/m3*	700
	Total surface area		*Branch_Area_FR*	*m2*	5,78
Trunk	Length		*Length_Trunk*	*m*	10
	dbh		*Diam_Trunk*	*m*	0,0859
	Apoplasmic fraction		*Trunk_apo_fraction*	*%*	0,4
	Symplasmic fraction		*Trunk_symp_fraction*	*%*	0,2
	Sapwood fraction		*Trunk_sapwood_fraction*	*%*	0,33
	Total surface area		*Trunk_Area_FR*	*m2*	2,69
Root	Fine roots length		*Length_Root_fi*	*m*	1114,08
	Fine roots end diameter		*Diam_Root*	*m*	0,001
	Apoplasmic fraction		*Root_apo_fraction*	*%*	0,4
	Symplasmic fraction		*Root_symp_fraction*	*%*	0,2
	Total roots length		*Length_Root_FR*	*m*	3835,79
	Total fine roots surface area		*Root_Area_FR*	*m2*	18,04
	Total roots surface area		*Root_Area_fi_0*	*m2*	3,5
	Root distribution	upper soil layer	*Root_upper*	2,5	2,5
		middle soil layer	*Root_middle*	0,4	0,4
		lower soil layer	*Root_lower*	0,1	0,1
	Root interface gap factor		*gap*	-	0
Water reservoirs	Branch symplasmic reservoir		*Q_Branch_Symp_FR*	*kg*	2,43
	Branch apoplasmic reservoir		*Q_Branch_Apo_FR*	*kg*	4,85
	Trunk symplasmic reservoir		*Q_Trunk_Sym_FR*	*kg*	6,39
	Trunk apoplasmic reservoir		*Q_Trunk_Apo_FR*	*kg*	12,77
	Root symplasmic reservoir		*Q_Root_Symp_FR*	*kg*	1,98
	Root apoplasmic reservoir		*Q_Root_Apo_FR*	*kg*	3,95
Stomatal and epidermal conductances	Canopy aerodynamic conductance		*g_crown0*	*mmol/s/m2*	45
	Maximum stomatal conductance		*gs_max*	*mmol/s/m2*	200
	Nocturnal stomatal conductance		*gs_night*	*mmol/s/m2*	20
	Parameter for stomatal response to PAR		*Jarvis_PAR*	-	0,006
	Temperature for maximal gs_max		*Tgs_optim*	*°C*	25
	Sensitivity of gs_max to temperature		*Tgs_sens*	-	17
	Cuticular conductance at 20°C		*g_cuti_20*	*mmol/s/m2*	3
	Phase transition temperature		*TP*	*°C*	37,5
	Q10 below TP		*Q10_1*	-	1,2
	Q10 above TP		*Q10_2*	-	4,8

Table 7 (continued)

Parameters			Name in SurEau	Unit	Value
	Branch epidermal conductance		*g_Branch*	*mmol/s/m2*	3
	Trunk epidermal conductance		*g_Trunk*	*mmol/s/m2*	3
	Root epidermal conductance		*g_Root*	*mmol/s/m2*	1
	Soil surface conductance at soil saturation		*g_Soil0*	*mmol/s/m2*	30
	Regulation parameter for gs		*Regul_gs_para1*	-	0,415
Hydraulic conductances	Branch apoplasmic conductance		*K_Branch_Apo_FR*	*mmol/s/MPa*	82,56
	Trunk apoplasmic conductance		*K_Trunk_Apo_FR*	*mmol/s/MPa*	394,42
	Root apoplasmic conductance		*K_Root_Apo_FR*	*mmol/s/MPa*	3570,78
	Leaf apoplasmic specific conductance		*K_Leaf_Apo0*	*mmol/s/MPa/m2*	5
	Terminal branch apoplasmic specific conductivity		*K_Branch_Apo0*	*mmol/s/MPa/m*	5000
	Trunk apoplasmic specific conductivity		*K_Trunk_Apo0*	*mmol/s/MPa/m*	50000
	Terminal root apoplasmic specific conductivity		*K_Root_Apo0*	*mmol/s/MPa/m*	25000
	Leaf symplasmic specific conductance		*K_Leaf_Symp_0*	*mmol/s/MPa/m2*	1,8
	Branch symplasmic specific conductance		*K_Branch_Symp0*	*mmol/s/MPa/m2*	1
	Trunk symplasmic specific conductance		*K_Trunk_Symp0*	*mmol/s/MPa/m2*	1
	Root symplasmic specific conductance		*K_Root_Symp0*	*mmol/s/MPa/m2*	1,4
Hydraulic capacitances	Leaf specific apoplasmic capacitance		*C_Leaf_Apo*	*Kg/MPa/dm3*	1,00E-04
	Branch specific apoplasmic capacitance		*C_Branch_Apo*	*Kg/MPa/dm3*	5,00E-06
	Trunk specific apoplasmic capacitance		*C_Trunk_Apo*	*Kg/MPa/dm3*	1,00E-05
	Root specific apoplasmic capacitance		*C_Root_Apo*	*Kg/MPa/dm3*	6,00E-04
Pressure Volume curves	Modulus of elasticity	Leaf symplasm	*Epsilon_Leaf_Symp*	*MPa*	10
		Branch symplasm	*Epsilon_Branch_Symp*	*MPa*	10
		Trunk symplasm	*Epsilon_Trunk_Symp*	*MPa*	10
		Root symplasm	*Epsilon_Root_Symp*	*MPa*	10
	Osmotic potential at full turgor	Leaf symplasm	*Pi0_Leaf_Symp*	*MPa*	-2,1
		Branch symplasm	*Pi0_Branch_Symp*	*MPa*	-1
		Trunk symplasm	*Pi0_Trunk_Symp*	*MPa*	-1
		Root symplasm	*Pi0_Root_Symp*	*MPa*	-1
Cavitation curves	P50	Leaf apoplasm	*P50_Leaf_Apo*	*MPa*	-3,4
		Branch apoplasm	*P50_Branch_Apo*	*MPa*	-3,4
		Trunk apoplasm	*P50_Trunk_Apo*	*MPa*	-3,4
		Root apoplasm	*P50_Root_Apo*	*MPa*	-3,4
	Slope	Leaf apoplasm	*Slope_Leaf_Apo*	*%/MPa*	60
		Branch apoplasm	*Slope_Branch_Apo*	*%/MPa*	60
		Trunk apoplasm	*Slope_Trunk_Apo*	*%/MPa*	60
		Root apoplasm	*Slope_Root_Apo*	*%/MPa*	60
Cavitation legacy	Legacy of PLC	Leaf apoplasm	*leg_Leaf*	-	0
		Branch apoplasm	*leg_Branch*	-	0
		Trunk apoplasm	*leg_Trunk*	-	0
		Root apoplasm	*leg_Root*	-	0

Acknowledgements HC would like to thank Nathalie Bréda and André Granier for their help in digging up experimental data from another millennium.

Funding This study was funded by the ANR projects 16-IDEX-0001 and 18-CE20-0005.

Data availability The C code of SurEau v. 20-12-26 used for this study (Cochard 2020b) is available from the data INRAE public repository: https://data.inrae.fr/dataset.xhtml?persistentId=doi:10.15454/6Z1MXK. The Preprint version of this article is available in the bioRxiv server (Cochard 2020a), doi: https://doi.org/10.1101/2020.05.10.086678

Declarations

Conflict of interest The authors declare no competing interests.

Open Access This article is licensed under a Creative Commons Attribution 4.0 International License, which permits use, sharing, adaptation, distribution and reproduction in any medium or format, as long as you give appropriate credit to the original author(s) and the source, provide a link to the Creative Commons licence, and indicate if changes were made. The images or other third party material in this article are included in the article's Creative Commons licence, unless indicated otherwise in a credit line to the material. If material is not included in the article's Creative Commons licence and your intended use is not permitted by statutory regulation or exceeds the permitted use, you will need to obtain permission directly from the copyright holder. To view a copy of this licence, visit http://creativecommons.org/licenses/by/4.0/.

References

Adams HD, Zeppel MJB, Anderegg WRL, Hartmann H, Landhäusser SM, Tissue DT, Huxman TE, Hudson PJ, Franz TE, Allen CD, Anderegg LDL, Barron-Gafford GA, Beerling DJ, Breshears DD, Brodribb TJ, Bugmann H, Cobb RC, Collins AD, Dickman LT, Duan H, Ewers BE, Galiano L, Galvez DA, Garcia-Forner N, Gaylord ML, Germino MJ, Gessler A, Hacke UG, Hakamada R, Hector A, Jenkins MW, Kane JM, Kolb TE, Law DJ, Lewis JD, Limousin JM, Love DM, Macalady AK, Martínez-Vilalta J, Mencuccini M, Mitchell PJ, Muss JD, O'Brien MJ, O'Grady AP, Pangle RE, Pinkard EA, Piper FI, Plaut JA, Pockman WT, Quirk J, Reinhardt K, Ripullone F, Ryan MG, Sala A, Sevanto S, Sperry JS, Vargas R, Vennetier M, Way DA, Xu C, Yepez EA, McDowell NG (2017) A multi-species synthesis of physiological mechanisms in drought-induced tree mortality. Nat Ecol Evol 1:1285–1291. https://doi.org/10.1038/s41559-017-0248-x

Blackman CJ, Pfautsch S, Choat B, Delzon S, Gleason SM, Duursma RA (2016) Toward an index of desiccation time to tree mortality under drought. Plant Cell Environ 39:2342–2345. https://doi.org/10.1111/pce.12758

Bréda N, Cochard H, Dreyer E, Granier A (1993a) Field comparison of transpiration, stomatal conductance and vulnerability to cavitation of Quercus petraea and Quercus robur under water stress. Ann Sci For 50:571–582

Bréda N, Cochard H, Dreyer E, Granier A (1993b) Water transfer in a mature oak stand (Quercus petraea). Seasonal evolution and effects of a severe drought. Can J For Res 23:1136–1143

Brodribb TJ, Cochard H, Dominguez CR (2019) Measuring the pulse of trees; using the vascular system to predict tree mortality in the 21st century. Conserv Physiol 7(1):coz046

Brodribb TJ, Powers J, Cochard H, Choat B (2020) Hanging by a thread? Forests and drought. Science 368:261–266

Cheaib A, Badeau V, Boe J, Chuine I, Delire C, Dufrêne E, François C, Gritti ES, Legay M, Pagé C, Thuiller W, Viovy N, Leadley P (2012) Climate change impacts on tree ranges: model intercomparison facilitates understanding and quantification of uncertainty. Ecol Lett 15:533–544. https://doi.org/10.1111/j.1461-0248.2012.01764.x

Christoffersen BO, Gloor M, Fauset S, Fyllas NM, Galbraith DR, BakerTR KB, Rowland L, Fisher RA, Binks OJ, Sevanto S, Xu C, Jansen S, Choat B, Mencuccini M, NG MD, Meir P (2016) Linking hydraulic traits to tropical forest function in a size-structured and trait-driven model (TFS v.1-Hydro). Geosci Model Dev 9:4227–4255. https://doi.org/10.5194/gmd-9-4227-2016

Cochard H (2020a) A new mechanism for tree mortality due to drought and heatwaves. bioRxiv, 531632, ver. 2 peer-reviewed and recommended by PCI Forest and Wood Sciences. doi: https://doi.org/10.1101/531632

Cochard H (2020b) Source code for SurEau.c, [dataset], Data INRAE repository, V2, 10.15454/6Z1MXK

Cochard H, Bréda N, Granier A, Aussenac G (1992) Vulnerability to air embolism of three european oak species (Quercus petraea (Matt) Liebl, Q. pubescens Willd, Q robur L). Ann Sci For 49:225–233

Cruiziat P, Cochard H, Améglio T (2002) The hydraulic architecture of trees: main concepts and results. Ann For Sci 59:723-752

Dayer S, Herrera JC, Dai Z, Burlett R, Lamarque LJ, Delzon S, Dortolomi G, Cochard H, Gambetta GA (2020) The sequence and thresholds of leaf hydraulic traits underlying grapevine varietal differences in drought tolerance. J Exp Bot (in press) 71:4333–4344

De Cáceres M, Martínez-Vilalta J, Coll L, Llorens P, Casals P, Poyatos R, Pausas JG, Brotons L (2015) Coupling a water balance model with forest inventory data to predict drought stress: the role of forest structural changes vs. climate changes. Agric For Meteorol 213:77–90. https://doi.org/10.1016/j.agrformet.2015.06.012

De Cáceres M, Mencuccini M, Martin-StPaul N, Limousin JM, Coll L, Poyatos R, Cabon A, Granda V, Forner A, Valladares F, Martínez-Vilalta J (2021) Unravelling the effect of species mixing on water use and drought stress in Mediterranean forests: a modelling approach. Agric For Meteorol 296:108233. https://doi.org/10.1016/j.agrformet.2020.108233

Domec JC, Smith DD, McCulloh KA (2017) A synthesis of the effects of atmospheric carbon dioxide enrichment on plant hydraulics: implications for whole-plant water use efficiency and resistance to drought. Plant Cell Environ 40:921–937. https://doi.org/10.1111/pce.12843

Dufour-Kowalski S, Courbaud B, Dreyfus P, Meredieu C, De Coligny F (2012) Capsis: an open software framework and community for forest growth modelling. Ann Sci For 69:221–233

Dutykh D (2016) How to overcome the Courant-Friedrichs-Lewy condition of explicit discretizations? arXiv preprint arXiv:1611.09646

Duursma RA, Blackman CJ, Lopéz R, Martin-StPaul NK, Cochard H, Medlyn BE (2019) On the minimum leaf conductance: its role in models of plant water use, and ecological and environmental controls. New Phytol 221:693–705

Eller CB, Rowland L, Oliveira RS, Bittencourt PRL, Barros FV, Da Costa ACL, Meir P, Friend AD, Mencuccini M, Sitch S, Cox P (2018) Modelling tropical forest responses to drought and El Niño with a stomatal optimization model based on xylem hydraulics. Philos Trans R Soc B Biol Sci 373. https://doi.org/10.1098/rstb.2017.0315

Fan L, Wigneron J-P, Xiao Q, al-Yaari A, Wen J, Martin-StPaul N, Dupuy JL, Pimont F, al Bitar A, Fernandez-Moran R, Kerr YH (2018) Evaluation of microwave remote sensing for monitoring live fuel moisture content in the Mediterranean region. Remote Sens Environ 205:210–223. https://doi.org/10.1016/j.rse.2017.11.020

Gentine P, Guérin M, Uriarte M, Mcdowell NG, Pockman WT (2016) An allometry-based model of the survival strategies of hydraulic failure and carbon starvation. Ecohydrology 9:529–546. https://doi.org/10.1002/eco.1654

Granier A, Breda N, Biron P, Villette S (1999) A lumped water balance model to evaluate duration and intensity of drought constraints in forest stands. Ecol Model 116:269–283

Hölttä T, Cochard H, Nikinmaa E, Mencuccini M (2009) Capacitive effect of cavitation in xylem conduits: results from a dynamic model. Plant Cell Environ 32:10–21. https://doi.org/10.1111/j.1365-3040.2008.01894.x

Huang CW, Domec JC, Ward EJ, Duman T, Manoli G, Parolari AJ, Katul GG (2017) The effect of plant water storage on water fluxes within the coupled soil–plant system. New Phytol 213:1093–1106. https://doi.org/10.1111/nph.14273

Jarvis PG (1976) The interpretation of the variations in leaf water potential and stomatal conductance found in canopies in the field. Philos Trans R Soc London, Ser B 273:593–610

Jones HG (2013) Plants and microclimate: a quantitative approach to environmental plant physiology. Cambridge university press

Kennedy D, Swenson S, Oleson KW, Lawrence DM, Fisher R, Lola da Costa AC, Gentine P (2019) Implementing plant hydraulics in the community land model, version 5. J Adv Model Earth Syst 11:485–513. https://doi.org/10.1029/2018MS001500

Klein T, Ramon U (2019) Stomatal sensitivity to CO2 diverges between angiosperm and gymnosperm tree species. Funct Ecol 33:1411–1424. https://doi.org/10.1111/1365-2435.13379

Lamarque LJ, Delzon S, Toups H, Gravel AI, Corso D, Badel E, Burlett R, Charrier G, Cochard H, Jansen S, King A, Torres-Ruiz JM, Pouzoulet J, Cramer GR, Thompson AJ, Gambetta GA (2020) Over-accumulation of abscisic acid in transgenic tomato plants increases the risk of hydraulic failure. Plant Cell Environ 43:548–562

Li L, Yang Z, Matheny AM, Zheng H, Swenson SC, Lawrence DM, Barlage M, Yan B, McDowell NG, Leung LR (2021) Representation of plant hydraulics in the Noah-MP land surface model: model development and multi-scale evaluation. J Adv Model Earth Syst 13. https://doi.org/10.1029/2020ms002214

Lopez R, Cano FJ, Martin-StPaul N, Cochard H, Choat B (2021) Coordination of stem and leaf traits define different strategies to regulate water loss and tolerance ranges to aridity. New Phytol 230:497–509. https://doi.org/10.1111/nph.17185

Loranty MM, Mackay DS, Ewers BE, Traver E, Kruger EL (2010) Competition for light between individual trees lowers reference canopy stomatal conductance: Results from a model 115. https://doi.org/10.1029/2010JG001377

Mackay DS, Ewers BE, Loranty MM, Kruger EL, Samanta S (2012) Bayesian analysis of canopy transpiration models: a test of posterior parameter means against measurements. J Hydrol 432-433:75–83. https://doi.org/10.1016/j.hydrol.2012.02.019.4

Mantova M, Menezes-Silva PE, Badel E, Cochard H, Torres-Ruiz JM (2021) The interplay of hydraulic failure and cell vitality explains tree capacity to recover from droughtPhysiol. Plant (in press) DOI 172:247–257. https://doi.org/10.1111/ppl.13331

Marino E, Yebra M, Guillén-Climent M, Algeet N, Tomé JL, Madrigal J, Guijarro M, Hernando C (2020) Investigating live fuel moisture content estimation in fire-prone shrubland from remote sensing using empirical modelling and RTM simulations. Remote Sens 12:2251. https://doi.org/10.3390/rs12142251

Martinez-Vilalta J, Anderegg WRL, Sapes G, Sala A (2019) Greater focus on water pools may improve our ability to understand and anticipate drought-induced mortality in plants. New Phytol 223:22–32. https://doi.org/10.1111/nph.15644

Martin-StPaul N, Delzon S, Cochard H (2017) Plant resistance to drought depends on timely stomatal closure. Ecol Lett 20:1437–1447

Martin-StPaul N, Ruffault J, Blackmann C, Cochard H, De CM, Delzon S, Dupuy JL, Lamarque L, Moreno M, Parsell R, Pimont F, Ourcival J, Torres-Ruiz J, Limousin J (2020) Modelling live fuel moisture content at leaf and canopy scale under extreme drought using a lumped plant hydraulic model. BioArxiv. https://doi.org/10.1101/2020.06.03.127167

Matheny AM, Bohrer G, Garrity SR, Morin TH, Howard CJ, Vogel CS (2015) Observations of stem water storage in trees of opposing hydraulic strategies. Ecosphere 6:1–13. https://doi.org/10.1890/ES15-00170.1

McDowell NG, Brodribb TJ, Nardini A (2019) Hydraulics in the 21st century. New Phytol 224:537–542. https://doi.org/10.1111/nph.16151

Mencuccini M, Manzoni S, Christoffersen B (2019) Modelling water fluxes in plants: from tissues to biosphere. New Phytol 222:1207–1222. https://doi.org/10.1111/nph.15681

Morin X, Bugmann H, de Coligny F, Martin-StPaul N, Cailleret M, Limousin JM, Ourcival JM, Prevosto B, Simioni G, Toigo M, Vennetier M, Catteau E, Guillemot J (2021) Beyond forest succession: a gap model to study ecosystem functioning and tree community composition under climate change. Funct Ecol 955–975:955–975. https://doi.org/10.1111/1365-2435.13760

Pimont F, Ruffault J, Martin-StPaul NK, Dupuy J-L (2019) Why is the effect of live fuel moisture content on fire rate of spread underestimated in field experiments in shrublands? Int J Wildland Fire 28:127. https://doi.org/10.1071/WF18091

Rambal S (1984) Water-balance and pattern of root water-uptake by a *Quercus-coccifera* L evergreen shrub. Oecologia 62:18–25

Ruffault J, Martin-StPaul N, Rambal S, Mouillot F (2013) Differential regional responses in drought length, intensity and timing to recent climate changes in a Mediterranean forested ecosystem. Clim Chang 117:103–117. https://doi.org/10.1007/s10584-012-0559-5

Ruffault J, Martin-StPaul N, Pimont F, Dupuy J-L (2018) How well do meteorological drought indices predict live fuel moisture content (LFMC)? An assessment for wildfire research and operations in Mediterranean ecosystems. Agric For Meteorol 262:391–401. https://doi.org/10.1016/j.agrformet.2018.07.031

Scoffoni C, Albuquerque C, Cochard H, Buckley TN, Fletcher LR, Caringella MA, Bartlett M, Brodersen C, Jansen S, McElrone A, Sack L (2018) The causes of leaf hydraulic vulnerability and its influence on gas exchange in Arabidopsis thaliana. Plant Physiol 178:1584–1601

Sinoquet H, Le Roux X, Adam B, Ameglio T, Daudet FA (2001) RATP: a model for simulating the spatial distribution of radiation absorption, transpiration and photosynthesis within canopies: application to an isolated tree crown. Plant Cell Environ 24:395–406

Sperry JS, Adler FR, Campbell GS, Comstock JC (1998) Limitation of plant water use by rhizosphere and xylem conductances: results from a model. Plant Cell Environ 21:347–359

Sperry JS, Venturas MD, Todd HN, Trugman AT, Anderegg WRL, Wang Y, Tai X (2019) The impact of rising CO2 and acclimation on the response of US forests to global warming. Proc Natl Acad Sci U S A 116:25734–25744. https://doi.org/10.1073/pnas.1913072116

Steppe K, De Pauw DJW, Lemeur R, Vanrolleghem PA (2006) A mathematical model linking tree sap flow dynamics to daily stem diameter fluctuations and radial stem growth. Tree Physiol 26:257–273

Tramblay Y, Koutroulis A, Samaniego L, Vicente-Serrano SM, Volaire F, Boone A, Le Page M, Llasat MC, Albergel C, Burak S, Cailleret M, Kalin KC, Davi H, Dupuy JL, Greve P, Grillakis M, Hanich L, Jarlan L, Martin-StPaul N, Martínez-Vilalta J, Mouillot F, Pulido-Velazquez D, Quintana-Seguí P, Renard D, Turco M, Türkeş M, Trigo R, Vidal JP, Vilagrosa A, Zribi M, Polcher J (2020) Challenges for drought assessment in the Mediterranean region under future climate scenarios. Earth-Science Rev 210:103348. https://doi.org/10.1016/j.earscirev.2020.103348

Tuzet A, Granier A, Betsch P, Peiffer M, Perrier A (2017) Modelling hydraulic functioning of an adult beech stand under non-limiting soil water and severe drought condition. Ecol Model 348:56–77. https://doi.org/10.1016/j.ecolmodel.2017.01.007

Tyree MT, Hammel HT (1972) The measurement of the turgor pressure and the water relations of plants by the pressure-bomb technique. J Exp Bot 23:267–282. https://doi.org/10.1093/jxb/23.1.267

Tyree MT, Yang S (1990) Water-storage capacity of Thuja, Tsuga and Acer stems measured by dehydration isotherms - the contribution of capillary water and cavitation. Planta 182:420–426. https://doi.org/10.1007/BF02411394

Van Genuchten MT (1980) A closed-form equation for predicting the hydraulic conductivity of unsaturated soils. Soil Sci Soc J 44:892–898

Venturas MD, Sperry JS, Love DM, Frehner EH, Allred MG, Wang Y, Anderegg WRL (2018) A stomatal control model based on optimization of carbon gain versus hydraulic risk predicts aspen sapling responses to drought. New Phytol 220:836–850

Walker AP, De Kauwe MG, Bastos A, Belmecheri S, Georgiou K, Keeling R, ... Zuidema PA (2020) Integrating the evidence for a terrestrial carbon sink caused by increasing atmospheric CO2. New Phytologist. (in press)

William PWA, Allen C, Macalady AK, Griffin D, Woodhouse CA, Meko DM, Swetnam TW, Rauscher SA, Seager R, Grissino-Mayer HD, Dean JS, Cook ER, Gangodagamage C, Cai M, McDowell NG (2013) Temperature as a potent driver of regional forest drought stress and tree mortality. Nat Clim Chang **3**:292–297. https://doi.org/10.1038/nclimate1693

Xu X, Medvigy D, Powers JS, Becknell JM, Guan K (2016) Diversity in plant hydraulic traits explains seasonal and inter-annual variations of vegetation dynamics in seasonally dry tropical forests. New Phytol 212:80–95. https://doi.org/10.1111/nph.14009

Yan B, Mao J, Dickinson RE, Thornton PE, Shi X, Ricciuto DM, Warren JM, Hoffman FM (2020) Modelling tree stem-water dynamics over an Amazonian rainforest. Ecohydrology 13:1–19. https://doi.org/10.1002/eco.2180

Publisher's note Springer Nature remains neutral with regard to jurisdictional claims in published maps and institutional affiliations.